Continental Shelf Research 175 (2019) 127–146

Contents lists available at ScienceDirect

Continental Shelf Research

journal homepage: www.elsevier.com/locate/csr

Research papers

Characterizing the vertical distribution of chlorophyll *a* in the German Bight

Changjin Zhao[a,*], Joeran Maerz[a,b], Richard Hofmeister[a], Rüdiger Röttgers[a], Kai Wirtz[a], Rolf Riethmüller[a], Corinna Schrum[a]

[a] Helmholtz-Zentrum Geesthacht, Institute for Coastal Research, Geesthacht, Germany
[b] Max Plank Institute for Meteorology, Hamburg, Germany

ARTICLE INFO

Keywords:
Vertical chlorophyll-a profiles
SCANFISH
Stratification
Turbulent mixing
Subsurface chlorophyll maximum layers
Resuspension
German Bight

ABSTRACT

Coastal and shelf seas display strong variability in the horizontal and vertical distributions of chlorophyll *a* (CHL). Detailed data are required to identify the processes that drive the observed spatio-temporal dynamics. A high-resolution, vertically resolved transect data set for biogeochemical and physical properties was collected in the inner German Bight (GB) from 2009 to 2011 on a seasonal basis. We used fluorescence as an indicator for phytoplankton biomass via the CHL concentrations. We classified profiles into different types by evaluating the heterogeneity of CHL vertical distribution and identifying vertical location (upper mixed layer, subsurface layer, bottom mixed layer of water column) of high CHL concentration in each profile. We analyzed the spatio-temporal occurrences of the different CHL vertical distribution types in the context of the hydrodynamic environment. More than half (68.7%) of all profiles showed vertically homogeneous CHL distributions. A smaller subset (3.2%) of all profiles showed subsurface CHL maximum layers (SCMLs) in the vicinity of the pycnocline, co-varying with strongly stratified conditions in deeper water. Profiles with highest concentration of CHL in the upper part of the water column (HCU) were observed in 11.5% of all profiles. Profiles with highest concentrations of CHL in the lower part of the water column (HCL) comprised 16.6% of all profiles. HCL profiles were extensively observed during the decay phase of the spring bloom and were associated with resuspension and erosion from pre-existing SCMLs, which could be driven by tide; photosynthetic activity below the pycnocline could also contribute. Under moderate weather conditions, tidal currents were the main driver of resuspension. This study highlighted the occurrence of SCMLs and HCL patterns in vertical CHL profiles in shallow shelf seas, such as the GB.

1. Introduction

Temporal and spatial variability in vertical chlorophyll a (CHL) distribution has long been recognized in temperate ocean waters (Boss and Behrenfeld, 2010; Herdman, 1923; Russell, 1927). The vertical distribution of CHL is shaped by a combination of biological processes, including the vertical patterns of growth and grazing influenced by the availability of light, nutrients and predators, and physical processes, such as mixing, resuspension and advection of plankton biomass (Riley, 1942). Surface sampling, e.g., via satellite images, limits the accurate description of the whole system (Charnock et al., 1993) and hampers the mechanistic understanding of the relation between environmental conditions and CHL distributions. Since the method of continuous vertical sampling of fluorescence as a proxy for CHL was introduced (Lorenzen, 1966), previously unappreciated features of the vertical distribution of CHL have been revealed. More than 20 years ago, strong heterogeneity in vertical CHL profiles, such as the occurrence of subsurface CHL maximum layers (SCMLs), has been found in the central and northern North Sea (Nielsen et al., 1993; Richardson and Pedersen, 1998). In the northern Dogger Bank area, recurrent and persistent SCMLs were suggested to significantly contribute to primary production (Fernand et al., 2013). The occurrence of SCMLs was attributed to bottom fronts, where injection of nutrients by tidal pumping supports primary production (Richardson et al., 2000; Weston et al., 2005). In stratified areas without frontal systems, hotspots of SCMLs were found to be related to local tidal mixing resulting from specific bottom bathymetry (Scott et al., 2010). We would expect considerable production in shelf seas contributed by SCML. However, limited estimations are able to confirm this based on available data. First, CHL:C (Chlorophyll a to carbon) ratio varies significantly in different time and spatial scales (Jakobsen and Markager, 2016; Wang et al., 2009). Second, phytoplankton tends to fluoresce more in autumn, when productivity is less due to lower light levels. and increasing light limitation (Kalaji et al., 2017). Third, SCML production also dependents on

* Corresponding author.
E-mail address: changjin.zhao@hzg.de (C. Zhao).

https://doi.org/10.1016/j.csr.2019.01.012
Received 28 February 2018; Received in revised form 16 January 2019; Accepted 27 January 2019
Available online 28 January 2019

injection of nutrients, which would be driven by physical process such as tidal stirring (Zhao et al., 2018) and baroclinic circulation (Pedersen, 1994).

In the southeastern North Sea, especially in the German Bight (GB), the vertical distribution of CHL has seldom been addressed since, as water depths are less than 40 m, tidal and wind-driven mixing were thought to homogenize the vertical CHL distribution at most times of the year. However, observations and simulations have shown stratification in the water column of the German Bight, which displayed an evident variability in extent, duration and intensity (Haren and Howarth, 2004; Pohlmann, 1996a, 1996b; Schrum, 1997). Apart from stratification, which potentially favors the development of SCMLs, other characteristic processes of the inner GB, such as the accumulation of settled detritus (Westernhagen et al., 1986) and low turn-over rates of organic matter (Beusekom and Brockmann, 1999), should further modify the vertical distribution of CHL and make it different from that in deeper areas. We herein investigate to which degree vertical heterogeneous CHL profiles develop and attribute their characteristics to coastal hydrodynamics and biogeochemical cycles.

Here we will employ high resolution transect data from the Coastal Observing System for Northern and Arctic Seas (COSYNA) (Baschek et al., 2017). Fluorescence profiles sampled in the COSYNA project throughout spring to autumn were used as proxy for CHL concentrations and we focused on vertical distribution pattern of CHL which are quantified within each profile. We are aware of the uncertainties resulting from varied fluorescence: CHL ratio; however, in general, the quantification of relative distribution of CHL within each profile, would not be influenced by those uncertainties. Afterwards, we characterize the seasonally variable vertical CHL patterns in the GB and examine potential mechanisms responsible for the observed vertical patterns. Our study thus provides a reference for the vertical CHL distribution in the GB. It will support the interpretation of observations and challenge coupled hydrodynamical-biogeochemical models for the GB in the future.

In this study, we attempt to provide answers to the following questions: (1) To what extent does the vertical CHL distribution show heterogeneity in the inner GB? (2) Are there any temporal and spatial patterns in the observed vertical CHL distribution that are related to the hydrodynamic environment or phytoplankton growth dynamics? Therefore, we first classified the vertical CHL profiles depending on whether relatively high concentrations of CHL were present in the upper or lower part of the water column and on the existence of a SCML. Next, we analyzed the spatial-temporal appearances of different vertical CHL profile types in the context of the seasonal dynamics of phytoplankton and stratification. Additionally, we investigated the potential biological and physical mechanisms responsible for the maintenance of observed SCMLs mainly via an empirical analysis. The potential factors responsible for the wide-spreading of higher CHL in the lower mixed layer, such as resuspension and erosion from a preexisting SCML, were also explored.

2. Observation data and methods

In this section, we first review the general hydrodynamic and biogeochemical conditions in our study area. Secondly, the data set and sampling methods and the pre-processing of the observational data are described. Thirdly, the detection of SCMLs and the classification of different types of vertical CHL distributions are laid out. In the fourth part, the characteristics of the CHL profiles, such as resuspension signals and CHL gradients in the deeper parts of profiles, are specified. To further analyze the occurrence of types of vertical CHL distributions with respect to the environmental setting, the irradiance, wind speed, and simulated hydrodynamic setting are introduced in the fifth part. To assess the tidal currents, which were not measured simultaneously, simulation results from a 3D hydrodynamic model were incorporated into this study after validation. The hydrodynamic processes potentially influencing the vertical CHL distribution pattern, such as tidal phases and stratification intensity were quantified.

2.1. Study site

The GB is a shallow area located in the southeastern part of the North Sea, with average water depth of approximately 25 m. The hydrodynamics are dominated by tides and wind forcing. The tidal amplitudes in the GB range from 1.8 to 3.4 m, with tidal currents of up to 0.6–1.0 m s^{-1} (Dietrich, 1950). In the near coastal areas of the GB, the water column is continuously mixed by tidal and wave forcing, which act against the seasonal thermal and haline stratification which is supported by the surface buoyancy induced by surface heat fluxes, riverine fresh water fluxes and tidal straining (Simpson et al., 1991). Further offshore, the surface heat flux competes with tidal stirring and generates seasonal thermal stratification (Czitrom et al., 1988). However, seasonal stratification can be interrupted by wind-driven mixing, even in summer. The interplay between the surface heat flux, wind/tidal mixing and river run-off regulates the mixing/stratification status in the GB (Dippner, 1993). The initiation and duration of continuous mixing and stratified conditions show high inter-annual variability (Schrum et al., 2003a, 2003b).

The inner GB exhibits high primary production (Joint and Pomroy, 1993). Driven by tidal and wave forces, resuspended materials are more frequently observed and remain in suspension longer in the southern part than in the northern part of the North Sea (Eisma and Kalf, 1987). The interactions between produced particulate organic matter and suspended sediments enhance aggregation and sinking (Maerz et al., 2016). The GB was suggested to be a temporal deposition area for organic matters, due to its high local productivity (Lohse et al., 1995) and its location in the northeastward transport routs of organic matter in the North Sea (Gehlen et al., 1995). Physical factors, such as frontal systems and estuarine circulation (Krause et al., 1986), also support primary production and confine the high turbidity, high nutrient concentrations and high primary production to the coastal area. The resuspension of settled organic matter containing CHL (Duineveld and Boon, 2002) due to shifts in the stratification/mixing status in the frontal zone (thereby modifying the intensity of vertical mixing) would further complicate the distribution pattern of CHL.

2.2. Sampling and pre-processing of data

High-resolution vertical transect data on biogeochemical and physical properties were provided by the observation project 'Coastal Observing System for Northern and Arctic Seas' (COSYNA) (Baschek et al., 2017). This observation project aimed at mapping interactions between physical and biological processes in the GB, where natural variability is influenced by anthropogenic and environmental changes. The vertical transect campaigns were repeated from 2009 to 2011 and covered most of the German Exclusive Economic Zone in the inner GB beyond 10 m water depth throughout spring to autumn. The observational data were sampled on ten cruises between 2009 and 2011 using the undulating towed system ScanFish Mark III™ (SCANFISH) connected to the RV Heincke (https://www.awi.de/en/expedition/ships/heincke.html) as part of the project "Coastal Observing System for Northern and Arctic Seas" (COSYNA: http://www.cosyna.de, Baschek et al., 2017). The research vessel sailed along a designated grid of east-west and north-south transects in the area of 3.5–8.3°E and 53.5–55.8°N that covered the German Exclusive Economic Zone in the GB (Fig. 1) and captured the across-shore gradients both off the East Frisian (north-south direction) and North Frisian (east-west direction) coast. The operation of the ship and the SCANFISH instrument required water depths deeper than 10 m and wind speeds less than 14 ms^{-1}. Sometimes, weather conditions prevented the completion of observations; the coverage of each cruise is listed below (Table 1). Further analysis was confined to profiles with valid profile depth no less than 10 m.

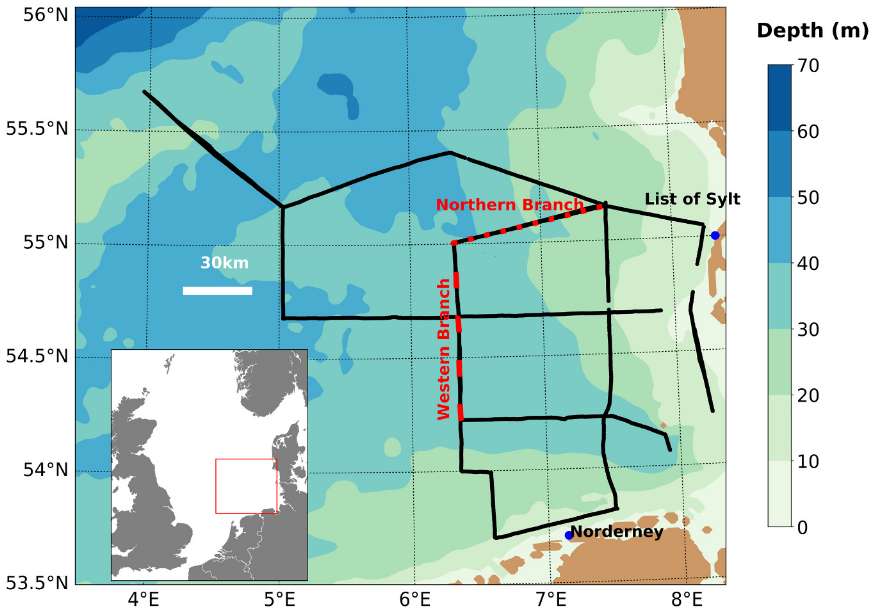

Fig. 1. Bathymetry in the German Bight and SCANFISH sampling transects (black lines). Dashed lines represent the repeatedly measured transects in July 2010 (cf. Section 3.3.3). The inset shows the North Sea and the GB location. The observation sites of surface irradiance, i.e., List on the island of Sylt and the island Norderney, are marked by blue dots.

Table 1
Basic information of the campaigns analyzed in this study.

Cruise number	Time	Wind speed ($m\,s^{-1}$)	Num. profiles(%)	Mileage (km)
303	2009.05.16–2009.05.25	6.6	5989(14.9)	1385
308	2009.07.28–2009.08.06	5.8	5491(13.6)	1281
312	2009.09.14–2009.09.20	8.1	4676(11.6)	920
319	2010.03.05–2010.03.11	8.2	5410(13.4)	1233
325	2010.05.02–2010.05.08	6.6	4566(11.3)	870
331	2010.07.13–2010.07.20	8.1	4870(12.1)	941
336	2010.09.19–2010.09.21	12.2	1164(2.9)	219
353	2011.04.06–2011.04.12	9.2	4850(12.0)	1111
359	2011.06.16–2011.06.19	7.4	1252(3.1)	608
365	2011.09.15–2011.09.19	8.7	2140(5.3)	561
Sum			40,408	9129

The ten cruises covered the growing seasons (spring, summer and autumn) in three consecutive years (Table 1), with similar spatial coverages in the majority of the cruises. Percentage of profiles measured in each campaign among all available profiles were laid out in the brackets behind the profile numbers. Thus, these data are suitable for investigating the seasonality using measured CHL profiles. Tidal phase was not considered in the planning of the cruises. The largely moderate wind conditions during the SCANFISH operation may have created a bias in stratification/mixing status, which is considered in the interpretation of the results.

The SCANFISH undulated 200–250 m behind the vessel and recorded vertical profiles along continuous V-curve paths, while maintaining safety margins of 3–5 m from the surface and the bottom. The vessel sailed at a speed of 6–8 knots. With a vertical speed of the SCANFISH of 0.4 $m\,s^{-1}$ and a sampling frequency of 11 s^{-1}, the vertical spacing between measurements was approximately 0.04 m. The horizontal span of each V curve ranged from 250 to 400 m, varying with the sailing speed of the vessel and the water depth. This sampling strategy provided simultaneous horizontal and vertical observations at a spatial resolution sufficiently high for the purposes of this study.

Among the multiple outputs provided by the sensors mounted on the SCANFISH, our analysis considered water pressure (PA-7, Keller AG, Switzerland), water temperature (PT100, ADM Elektronik, Germany - cruises 303–319; NTC sensor, ISW Wassermesstechnik, Germany - cruises 325–365), conductivity (Conductivity Sensor, ADM Elektronik, Germany), optical turbidity (Seapoint Turbidity Meter 880 nm, Seapoint Sensors Inc., USA), oxygen saturation level (Shallow Water Dissolved Oxygen Micro-Sensor, AMT Analysenmesstechnik GmbH, Germany), chlorophyll a fluorescence (TriOS MicroFlu-chl, TRIOS Inc., Germany). For the chlorophyll a fluorescence instrument, light source ultra-bright blue LED has peak wavelength at 470 nm; detection of peak wavelength is at 685 nm, with 20 nm of full width at half maximum. Optical attenuation coefficient was computed from transmission measurement at 660 nm (C-Star Transmissometer, WETLabs Inc., USA). Salinities and potential water densities (σ_t) were calculated using the international thermodynamic equation of seawater (McDougall et al., 2010; Millero et al., 2008). The sensitivity of the TRIOS fluorescence signal to turbidity was corrected as described in Maerz et al. (2016). TRIOS Inc. delivers the output of the TriOS MicroFlu-chl from raw fluorescence readings that were transferred to physical units calibrated a lab chlorophyll-a standard by a first order polynomial equation. The ratio between fluorescence and chlorophyll pigments is known to vary (Kiefer, 1973) by up to a factor of two or even more (Petersen et al., 2011). In the subsequent data analysis we used fluorescence as a proxy for phytoplankton biomass via the CHL concentrations. For the conversion we assumed a constant ratio between fluorescence and CHL (we call it F: CHL hereafter and use arbitrary unit of CHL as the unit of fluorescence signal). In general, we focus on the relative distribution of CHL in the water column; in another words, we quantified the vertical shape of each CHL-profile in terms of CHL concentration in one segment of water column being “higher than”, “lower than” or “comparable to” to other parts (upper, middle (pycnocline) and lower parts) of the same profile. No comparison was made among different profiles using absolute value. We are aware of the uncertainties resulting from varied fluorescence: CHL ratio and CHL: C ratio (Babin et al., 2008; Claustre et al., 1999). Relevant calibration and estimation of these uncertainties has been conducted to prove that the results would not be influenced by those uncertainties.

183 HPLC measured CHL data were sampled simultaneously during these campaigns. We made use of the available HPLC measured CHL data to estimate the varying range of F: CHL, in each season, each year and between different vertical segments (Appendix A). Influence of quenching on fluorescence profile in the surface water column has also been adjusted (Appendix A). Generally, F: CHL mainly lies in the range between 1 and 2; the seasonal and inter-annual variability also vary no more than a factor of 2. In addition, around 60% of the F: CHL’s variabilities between surface and subsurface segments of water column, are no more than factor of 2. In the following analysis, we took a variation

of factor 2 into account. For the profile classification we also choose this criteria, which exceeds the range of the uncertainty in the F:CHL ratio, to ensure that the difference in fluorescence reflects the difference of CHL, rather than resulting from the varied F: CHL ratio.

The data sets were binned along the observation curve into regular vertical blocks of 10 cm to avoid unevenly sampling. The consecutive data sets were split into up and down profiles. For all parameters except those relevant to oxygen, we used only downward profiles to keep the lag effects of the sensors systematically coherent. A comparison of subsequent downward and upward profiles of oxygen saturation exhibited a substantial lag in the oxygen signal, suggesting a time constant of several seconds in campaigns taken after 2009. This temporal lag corresponds to approximately 5 m in the vertical signals. Rather than detecting the accurate vertical location of the oxygen maximum, we focused on the relative positions of the oxygen maximum and the SCML, under the assumption that the lag effects are stable. Downward profiles covered a horizontal span ranging from 125 to 200 m. We assumed that the lateral change within this horizontal span was negligible and treated the V curves from downward profiles as being perpendicular to the seafloor. As the upper mixed layer generally extended 10 m or more downwards, any disturbances attributable to the ship's hull or quenching effects of CHL in the most uppermost meters should have a negligible impact on the profile classification.

All the binned data sets underwent low-pass Butterworth filtering (Butterworth, 1930) to remove short-term variations. Half of the resolution of the binned vertical step was set to be the higher constraint of the filter to avoid aliasing (Grenander, 1959). This process also damped out most of the artefacts in the computed salinities and water densities at the pycnocline caused by the thermal lag of the conductivity cells.

2.3. Classification of characteristic vertical CHL distribution types

To evaluate and compare the heterogeneity of vertical CHL profiles in a systematic way, we classified the measured CHL profiles into 6 characteristic types depending on whether a SCML was detectable and whether the CHL concentrations differed between the upper part and the lower part of the water column (Fig. 2). Following Dekshenieks et al. (2001), a SCML is defined as a subsurface CHL layer whose amplitude is distinctly higher than adjacent water columns and the thickness is relatively thin compared to whole water column; the characteristics in amplitude and thickness display persistence in reasonable temporal and spatial scales. Considering the transient and turbulent environmental conditions, as well as the notable variability in vertical CHL concentrations in our system, we modified these criteria to capture the layer features and to reflect the general character of SCMLs in our system. To select potential candidates for SCML in the profiles, we applied three steps: First, we identified points where the first-order derivative of the CHL profiles switched from positive to negative (Fig. A.3.b). Second, to identify the edges of a potential SCML, within 5 m of the potential layer peak, the local maxima in the second-order derivative of a CHL profile above and below the peak were assigned as the upper and lower edges of the SCML, respectively (Benoit-Bird et al., 2009) (Fig. A.3.c). Third, to evaluate the significance of the potential SCML, the amplitude of the peak was compared to the background value (Fig. A.3.a). We estimated the local background value by linearly interpolating the upper and lower edges' values to the depth of the peak. A SCML was only recognized if the candidate satisfied the 3 following threshold criteria. Criterion 1: To discard peaks resulting from local fluctuations, the peak amplitude of a potential SCML was required to be 2.5 times larger than the standard deviation of the CHL profiles within a 5 m extent upward and downward from the peak. Criterion 2: The peak value was required to be 2 times higher than the background value (Fig. A.3.a). Criterion 3: To exclude CHL layers with weak gradients, the relative CHL gradient above and below the peak was required to exceed 0.125 m^{-1}. Here, we used the relative gradient instead of the absolute gradient to exclude the effects of spatial variability in CHL amplitudes and to make it possible to process all profiles with the same threshold criteria. The relative gradient was calculated by dividing the CHL gradients between the peak and edges by the peak value.

Under the condition that a SCML was present, we divided the whole water column into 3 sublayers: an upper layer, a middle layer corresponding to the SCML and a lower layer. Otherwise, we divided the water column into sublayers depending on the difference in CHL concentrations between the upper and lower parts of the water column (Fig. A.4). We selected the depth corresponding to the maximum absolute difference between averaged CHL concentration above and below to split the whole water column into upper and lower parts (Fig. A.4.b). The difference in the CHL concentrations among the sublayers was quantified by the ratio between the sublayers (Fig. A.4.a). By applying this method, the spatial variability in CHL was also excluded and we could process all profiles using the same analysis criteria.

After we divided the water column into 3 (SCML present) or 2 (no SCML present) sublayers, we classified the CHL profiles into 6 groups depending on the CHL ratios among the sublayers. A complete flow chart of the profile classification method is presented in Fig. A.5. If the averaged CHL ratio between two sublayers was larger than 2 (Appendix A), the difference between the two sublayers was regarded as significant. The 6 types of vertical CHL profiles (Fig. 2) were then defined as follows. Type 1, SCM: A SCML was present, and the mean CHL concentration of the SCML was notably higher than that of the upper and lower parts of the water column. No significant difference in the mean CHL value between the upper and lower parts of the water column was present (Fig. 2a). Type 2, higher CHL concentrations in the lower layer (HCL): Relatively high CHL concentration was present in the lower part of the water column without the appearance of a SCML (Fig. 2b). Type 3, higher CHL concentrations in the upper layer (HCU): Relatively high CHL concentration was present in the upper part of the water column without the appearance of a SCML (Fig. 3c). Type 4, well-mixed (WM): Neither a SCML nor a significant difference in CHL concentrations between the upper and lower parts of the water column was found. In many profiles with a SCML, the upper or lower parts were not symmetric with respect to the subsurface layer; in other words, the mean CHL value in the SCML was significantly higher than that in one part but not the other. These profiles were classified as two transient types as follows (Fig. 2d). Type 5: The mean CHL value in the SCML was higher than that in the upper part of water column but not that in the lower part (SCM-HCL) (Fig. 2e). Type 6: The mean CHL value in the SCML was higher than that in the lower part of water column but not that in the higher part (SCM-HCU) (Fig. 2f).

To investigate the seasonality of vertical CHL distribution patterns, we binned profiles into 4 segments depending on water depth: 10–15 m, 15–25 m, 25–35 m, 35–45 m. We grouped the 10 campaigns into 4 growing seasons: early spring (319: March 2010; 353: April 2011), late spring (303: May 2009; 325: May 2010), summer (308: July-August 2009; 331: July 2010; 359: June 2011), and autumn (312: September 2009; 336: September 2010; 365: September 2010). The spring season was divided into early and late spring regarding to whether the spring bloom decayed, with reference to the surface CHL concentration estimates from remote sensing data (ESA Ocean Colour Climate Change Initiative (OC-CCI; http://www.esa-oceancolour-cci.org/) (Müller et al., 2015).

We performed several sensitivity analyses on our selection criteria. For the detection of SCMLs, we assessed the sensitivity of the second and third criteria introduced above. Among all profiles with SCML candidates (the first-order derivative of the CHL profile crosses 0 in water columns deeper than 5 m), the proportion of confirmed SCMLs stabilized at approximately 20% when the threshold of peak-background ratio was set between 1.125 and 1.7 and the relative gradient ranged from 0.05 to 0.2 m^{-1}. Fewer SCMLs are recognized with stronger criteria (with higher value), and vice versa. Based on the uncertainty analysis regarding the varied F: CHL, we have to choose the peak-

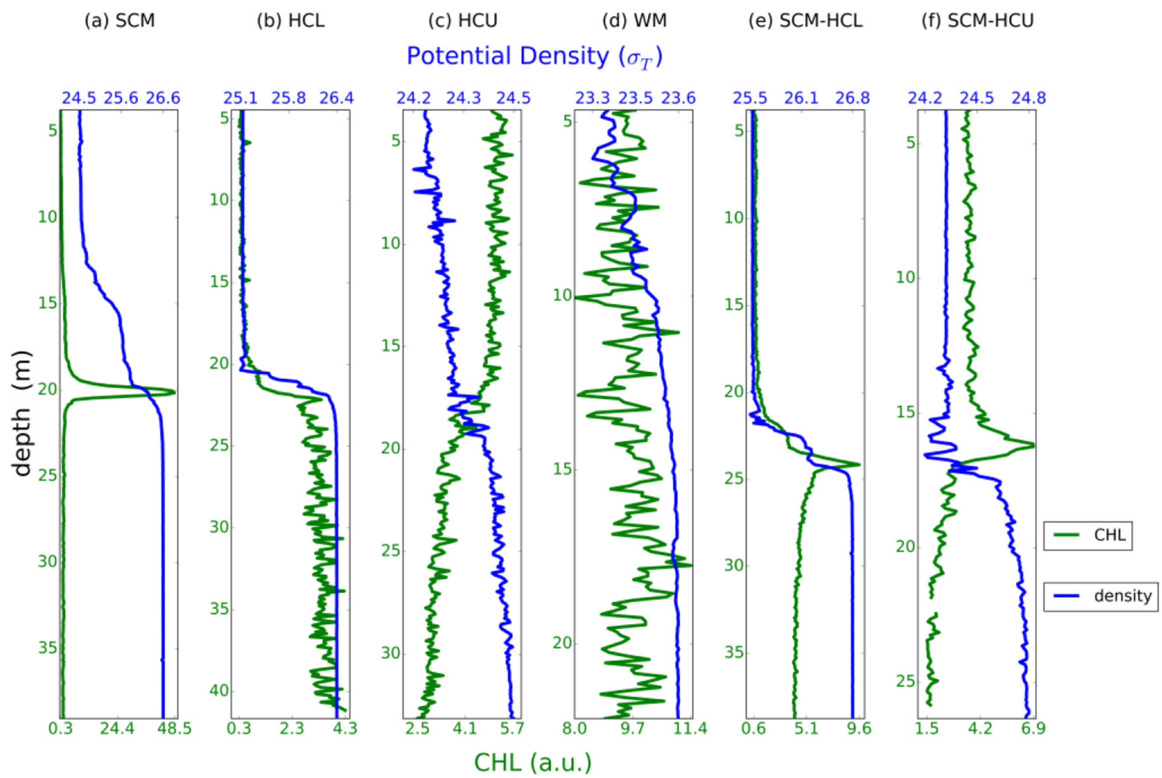

Fig. 2. Example CHL profiles. (a) SCM: Subsurface CHL maximum is detectable. No notable difference of CHL concentration between the upper and lower layer. (b) HCL: CHL concentration in the lower layer of the water column is higher than that in the upper layer. (c) HCU: CHL concentration in the upper layer of the water column is higher than that in the lower layer. (d) WM: Well-mixed CHL profile. (e) SCML-HCL: A subsurface CHL maximum layer is detectable and the averaged CHL concentration in the upper part of the water column is distinguishably lower than that in the lower part. (f) SCML-HCU: A subsurface CHL maximum layer is detectable and the averaged CHL concentration in the upper part of water column is distinguishably higher than that in the lower part.

background ratio as 2 to exclude the condition that the higher CHL indicated by fluorescence signal is due to the increase F: CHL in subsurface layer. When applied this criterion of peak-background ratio, among all potential SCMLs, 10% satisfied the threshold criterion. It indicates that the chosen criteria guaranteed the separation of SCMLs from background noise and, at the same time, ensured that the analysis remained selective.

To select the optimal critical ratio between sublayers, we varied the ratio of averaged CHL concentrations among sublayers from 1.5 to 2.5, with a step of 0.1. More profiles were classified as WM when higher critical ratios were used. Even if SCMLs were present, the profiles were more frequently identified as transient types, i.e., SCM-HCL and SCM-HCU, when higher critical ratios were applied. When we increased the critical ratio values to 1.8, the number of profiles classified into the 4 major types (SCM, HCL, HCU, and WM) was insensitive as it was for smaller critical values. , with the number of profiles changing by no more than 9%. Notably, the appearance of a SCML would not necessarily classify the profile as SCM if the mean CHL value in the SCML was not distinguishable from that of the other sublayers.

2.4. Quantify the resuspension signal in the bottom mixed layer

To investigate the source of high CHL concentrations in the lower mixed layer, we detected CHL peaks near the bottom (CPB) and CHL gradients in the deepest 5 m (CG5) in the CHL profiles to identify resuspension. There were two criteria for the detection of CPB: 1) The peak value in the bottommost 5 m should be at least 1.5 times higher than the average value in the lower layer. The mean value in the lower layer was used as a substitute for defined background values, which we have used for the detection of SCMLs since the layer bound detection possessed high uncertainty near the bottom. 2) The relative gradient had to be larger than $0.0625\,m^{-1}$. The calculation of the relative gradient was done in a similar way to that of SCMLs. CHL gradients in the deepest 5 m in CHL profiles (CG5) were calculated as follows: the averaged CHL value in the deepest 1.25 m in the profile was subtracted from the averaged CHL value in the deepest 5–7.5 m in the profile and then divided by the depth interval, which is 5 m here. Here, we adopted the average value of depth intervals rather than single points to minimize the bias caused by local spikes and discontinuities in profiles. Since many profiles presented an increasing trend downward instead of a sharp increase at the bottom, we also calculated the mean gradient of CHL in the lower part of the water column (in the SCM-HCL, HCL and SCM profiles), referred to as CGL for short, to represent the general CHL variation trend with depth. If the CHL concentration increased with depth, the gradients (CG5, CGL) mentioned above possess positive values, and if the CHL concentration decreased with depth, the opposite is true.

To further investigate the mechanism driving resuspension, we examined the occurrence of resuspension with respect to tidal phases. We counted the number of profiles belonging to tidal phase segments and the occurrence of resuspension signals (e.g., CPB) in the profiles. By dividing the number of profiles possessing resuspension signals by the number of profiles measured in each tidal-phase segment, we obtained the relative occurrence of resuspension for each tidal phase.

2.5. The physical environment

To analyze the vertical CHL distribution of profiles in the context of the environmental setting, we calculated the irradiance and turbulence as important physical factors for phytoplankton growth and distribution. We calculated euphotic layer depth and assessed stratification using observational data, as measured irradiance and density data were available. As no simultaneous measurements of turbulence were available, the following data from a 3D simulation were used:

dissipation rates ε, velocity shear S^2, kinematic viscosity ν, and current information. To ensure the consistency of our analysis, we also applied squared buoyancy frequency computed from simulated water density profiles to do validation of simulated data sets.

Euphotic layer depth: Euphotic layer depth is an indicator to quantify how deep the irradiance can penetrate and sustains photosynthesis. Here, we calculated the euphotic layer depth to examine whether irradiance is able to influence the SCML depth. We used short-wave radiation records and profiles of attenuation coefficients to calculate the irradiance profiles in the water column according to the Lambert-Beer law (Swinehart, 1962). Daily mean values of two surface short-wave radiation data time series were used to represent the average irradiance conditions for the GB. These two measuring stations for surface short wave radiation are located on Norderney and List on the island of Sylt (Fig. 1) at the southern and eastern border of the GB, respectively (DWD, 2015). The value of 7 W/m^2 was chosen (Brand and Guillard, 1981) as the lowest amount of irradiance necessary for the growth of phytoplankton, and we defined the euphotic layer depth as the depth where absolute irradiance values hit this threshold (Banse, 2004).

To better interpret the vertical distribution of CHL with respect to the hydrodynamic setting, we calculated some proxies to quantify the counteracting processes between mixing and stratification that may help initiate, maintain or undermine the vertically heterogeneous CHL structures. Here, we briefly outline the definitions and calculations of these proxies for the turbulent status, as used in previous analytical work (Steinbuck et al., 2010).

Squared buoyancy frequency: SCMLs and other vertical CHL patterns were often associated to the intensity of stratification. The intensity of stratification can be evaluated by squared Brunt-Väisälä or buoyancy frequency N^2, which is defined as follows:

$$N^2 = -\frac{g}{\rho_0}\frac{d\rho}{dz} \tag{1}$$

where g is the gravitational acceleration, ρ_0 is the averaged potential water density of the whole vertical profile, dz represents the vertical sampling step in binned data sets (10 cm) and ρ is the potential density value at each vertical bin in the profile. To categorize the vertical density profiles with respect to stratification status, we first selected the segments in each profile where N^2 exceeds 0.001 s^{-2} as pycnocline candidates. Among these pycnocline candidates, we merged segments if the distance between them was smaller than 0.5 m and neglected pycnocline candidates that were too thin (i.e., those with thicknesses of less than 1 m). These two steps were designed to exclude the impact of noise. As a final step, the selected and merged segments within the shallowest and deepest 5 m of the measured profiles were also discarded since the undulating motion of the vehicle could generate artificial gradients in the density profiles. Choosing this step-wise criterion allowed the detection of multiple pycnoclines, which have been observed in the GB. We used the observed potential water density to calculate N^2 here. To support the analysis of physical factors of the vertical CHL distribution, similar to the statistical processes applied to determine the seasonality of the vertical CHL distribution pattern, the occurrence of stratification was statistically grouped into segments by depth – 10–15 m, 15–25 m, 25–35 m, and 35–45 m – and into 4 seasons, as mentioned in Section 2.3 (Fig. 3).

Diffusion coefficient: Turbulent mixing can redistribute CHL concentrations between adjacent sublayers and undermine gradients in layers in which CHL potentially accumulates or grows. In our study, the diffusivity was calculated proportionally to the ratio between dissipation rate ε and squared buoyancy frequency (Osborn, 1980):

$$Kz = 0.2\frac{\varepsilon}{N^2} \tag{2}$$

Richardson number: Velocity shear counteracts the stabilizing effect of stratification. This competition is expressed by the gradient Richardson number:

$$Ri = N^2/S^2 \tag{3}$$

The critical gradient Richardsen number is Ri = 0.25. For Ri < 0.25 the flow is likely to remain turbulent (Kundu et al., 2016).

Buoyancy Reynolds number: The interplay between stratification and turbulence is quantified by the buoyancy.

$$Re_b = \varepsilon/(\nu N^2) \tag{4}$$

Reynolds number: When the Re_b is smaller than 15, stratification dominates. In contrast, turbulence is unaffected by stratification when the Re_b is greater than 100. When the Re_b ranges from 15 to 100, stratification is affected by turbulence (Monismith et al., 2018).

Simpson-Hunter parameter: The stability of stratification is quantified by the ratio between the cube of the mean tidal current speed $\bar{u}$ during one tidal cycle and the water depth h (Pingree and Griffiths, 1978; Simpson and Hunter, 1974)

$$SH = log_{10}(\bar{u}^3/h) \tag{5}$$

The Simpson-Hunter parameter indicates the tendency for a formerly stratified water column to become mixed. The larger the value is, the stronger the rates of tidal energy dissipation per unit mass are, and the easier the stratification can be disrupted.

Since only a limited number of the physical factors discussed above were simultaneously measured during the SCANFISH cruises, we obtained values for the turbulence dissipation rate ε, kinematic viscosity ν, squared shear S^2 and mean tidal velocity $\bar{u}$ from a 3D hydrodynamic simulation with the General Estuarine Transport Model (GETM) (Gräwe et al., 2015). By using vertically adaptive coordinates (Hofmeister et al., 2011), the vertical resolution of the computational layers increases at locations where strong stratification occurs, thus ensuring improved resolution of the spatial and temporal variability in stratification. The GETM set-up simulated the southern North Sea and Baltic Sea with a horizontal resolution of 1.8 km and 42 vertical layers. The model simulations covered the time span of all campaigns. We used output from the hindcast run, which was stored in snapshots every 2 h. We interpolated the model results linearly in time and space to obtain the corresponding hydrodynamic conditions for each measured data point.

Before further analysis, we ensured sufficient consistency between the simulated and observed density profiles. First, we binned the simulated data into 10 cm vertical resolution grids and extracted the pycnocline using the same method applied for the observed density profiles. Second, when stratification developed, we calculated the density gradients within the pycnocline to quantify the intensity of the stratification, for which the discrepancy between the observations and simulations should not exceed 0.015 σ_t m^{-1}. Further discussion of the physical conditions of SCMLs was restricted to profiles in which the simulation met the validation criterion.

3. Results and discussion

3.1. General hydrographic conditions during the cruises

In accordance with our criteria, among all analyzed downward profiles 54% were stratified. Stratification mainly emerged in campaigns 303 (May 2009), 331 (July 2010), and 359 (June 2011) when stratification was present in at least 80% of the profiles.

The seasonality of stratification has been revealed by the proportions of stratified profiles (Fig. 3). As noted by previous studies, the onset of thermal stratification occurs in late spring/early summer (Pohlmann, 1996a, 1996b). In the study area, haline stratification could superimpose mixing in regions with freshwater inflows (Simpson et al., 1991). In early spring, the proportion of stratified profiles was not more than 25%. The proportion of stratification peaked in June and began to drop in August. In autumn (September), proportion of stratification decreased down to approximately 50% of the profiles in deeper areas and only approximately 20% of the profiles in shallow areas. Due to the

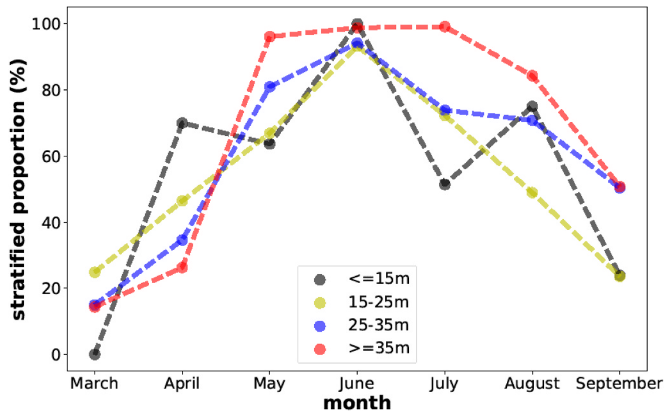

Fig. 3. Seasonality in stratification as revealed by the SCANFISH data. Density profiles are grouped for each month and depth segment; the corresponding stratified percentage is calculated.

rather moderate weather conditions during the sampling periods of the cruises, which is not necessarily representative (Geyer et al., 2015) in terms of the climatological conditions in longer time scales, we expected that the stratified proportions should be higher than the mean climatological conditions.

3.2. Seasonal characteristics of CHL profiles

Approximately 68.7% of all profiles showed a vertically homogeneous CHL distribution. The HCU type were observed in 11.5% of all profiles and the HCL type accounted for approximately 16.6% (Fig. 4). Only a small subset (1.9%) of all profiles were identified as the SCM type. The transient types SCM-HCL and SCM-HCU only represented a tiny proportion in the typology analysis, together accounting for 1.3%. We therefore merged these two transient types with the SCM type (in total accounting for 3.2%) in the following analysis of the seasonality of the vertical CHL profiles. We only separate these two transient types when transformation among different distribution types is discussed (cf. Section 3.4).

The proportions of the WM type corresponded to the seasonal stratification/mixing cycle (Fig. 3). They decreased starting in late spring, reached the lowest level in summer and increased again in autumn. More profiles displaying defined vertically heterogeneous CHL distributions were found in deeper areas. The SCM type only emerged under strong stratification, in summer, its proportion increased with water depth, from 2.0% in the 15–25 m region to 20.0% in regions deeper than 35 m. No SCM type appeared in areas shallower than 15 m. In other seasons, SCM profiles were rarely detected, with proportions no larger than 1.0%. In late spring, the HCL type dominated except for WM type, particularly in areas shallower than 15 m. In autumn, in addition to the increased occurrence of WM, the HCU type dominated in all depth segments except WM type, accounting for 26.7% in areas deeper than 35 m and approximately 2.2–15.2% in shallower areas. The occurrences of the SCM and HCL profiles decreased in autumn.

The high standard deviation in the seasonality of the CHL profile types (Fig. 4) can be attributed to the significant variability in our system and the availability of observed profiles in each season assessed in our study. In deeper regions (≥ 25 m), the appearance of SCM profiles varied among campaigns. In campaigns 331 (July 2010) and 359 (June 2011), the extensive distribution of SCM profiles was closely related to strong stratification; in contrast, in campaign 312 (August 2009), under strong mixing, few SCM profiles were detected, even in deeper areas.

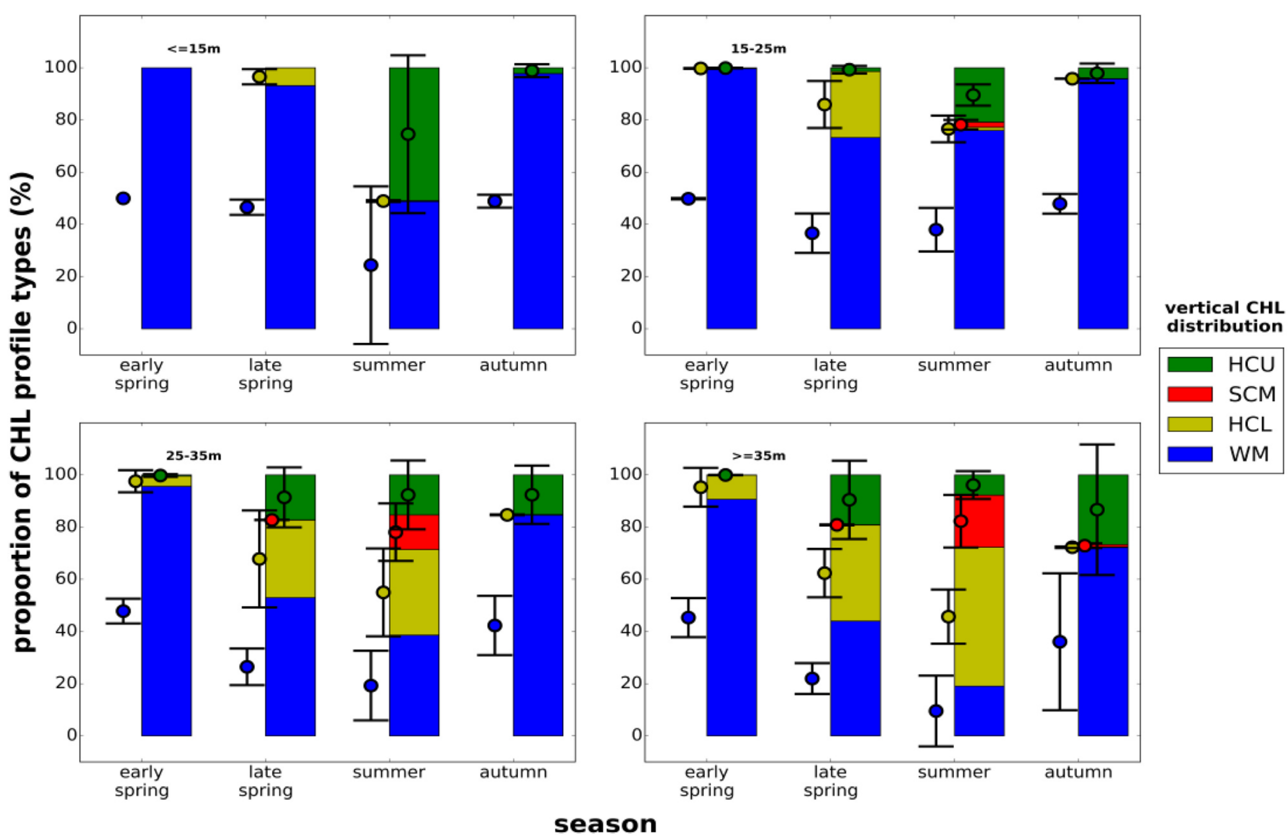

Fig. 4. Occurrences (in percent) of different CHL vertical distribution types in different water depth segments (shallow: 10–15 m, relatively shallow: 15–25 m, relatively deeper: 25–35 m, deep: 35–45 m). WM: well-mixed type. HCU: higher CHL mean concentration in the upper part of the water column than that in the lower part, without a SCML. HCL: higher CHL mean concentration in the lower part of water column than that in the upper part, without a SCML. SCML: subsurface CHL maximum layer. The transient types (SCM-HCU and SCM-HCB) are combined into the SCM type because of the emergence of SCML. Error bars represent standard deviations among cruises.

The SCM type also developed in moderately shallow regions (15–25 m) when strong stratification occurred (campaign 331: July 2010).

The occurrences of the HCU and HCL types also displayed substantial variability, especially in spring. The upper layer of the water column normally favors of phytoplankton growth in spring, due to higher availability of irradiance compared to that of the lower layer. However, higher CHL concentrations in the upper layer were not necessarily detectable in our observations because of the dilution resulting from vertical mixing in the water column. In addition, the proportions of HCU and HCL profiles in the late spring also depended on the variability in the decay phases of spring blooms in specific areas and onset time of stratification, even if we have grouped campaigns into seasonal groups based on the general flourishing patterns from satellite images. The CHL that sank down can remain suspended in the lower part of the water column and barried below the pycnocline.

3.3. Occurrence of subsurface CHL maximum layers (SCMLs)

3.3.1. Physical and biogeochemical characteristics of SCMLs

In a comparison of the stratification patterns among different water depth segments and seasons, the occurrence of SCMLs was basically in line with stratification, and the SCM type was detectable in summer and in deeper water, where stratification was observed in at least 66.8% of the profiles. The most extensive and notable SCMLs were observed in summer during campaigns 331 (July 2010) and 359 (June 2011). In these campaigns, SCMLs were present in 16.0–20.9% of the stratified water columns, with horizontal extents ranging from 50 km to 250 km. More than 90% of the SCMLs exhibited a thickness in the range of 4–6 m. In the SCMLs, the averaged CHL concentrations were primarily 3–9 a.u. and approximately 10% reached 10 a.u. The CHL concentration in the upper mixed layers was lower than that in the SCMLs, and more than 90% of surface layer concentrations were less than 2 a.u. In the calibration process, we found that the variation range of F: CHL is no more than factor 2. Considering the F: CHL's variation in the same profile, 66.7% of F: CHL(subsurface/surface) lies in between 0.5 and 2 (Table A1). If considering this variation, the peak value of fluorescence in Fig. 5a lies no more than 2 (a.u.), the indicated peak value of CHL should be no more than 4 (a.u.). The disparity is not as large as the raw fluorescence data has indicated but we can still expect that the CHL value in the SCML is higher than that in the upper layer. The averaged CHL concentration in the lower mixed layer was distinctly higher than that in the upper mixed layer, which we will address further in Section 3.4.

The characteristics of the physical environment and the CHL concentrations in all profiles with detectable SCMLs are summarized in Fig. 5. SCMLs were only detected within pycnoclines with stable stratification and physical conditions in the pycnoclines were distinct from those in the layers above and below (Fig. 5). The flow within the pycnocline was typically stable (Ri > 1/4, Fig. 5f) and the buoyancy Reynolds numbers were smaller than 15. The vertical diffusivity K_z was primarily in the range 10^{-6} - 10^{-5} m^2s^{-1} within the pycnocline. Shear instability (Ri < 1/4) was present in the lower mixed layer in more than half of the profiles and in the upper mixed layer in 10% of the profiles. Compared to the turbulence in the pycnocline, the turbulence in the upper mixed layers was stronger, but these layers were still dominated by stratification (Re_b < 15). In the lower mixed layers,

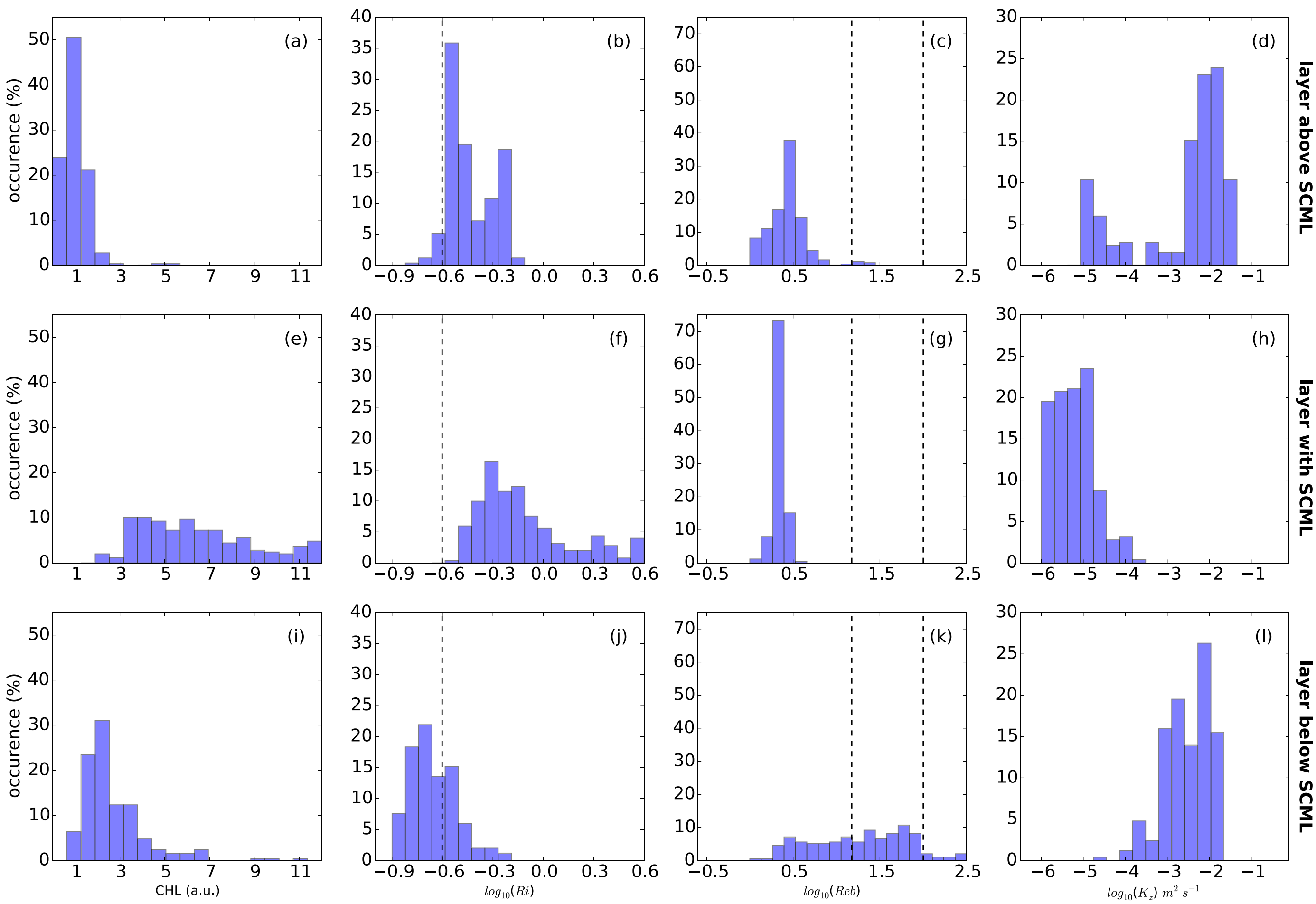

Fig. 5. Histograms of vertically averaged CHL concentration, log_{10}-transformed Richardson number R_i, buoyancy Reynolds number Re_b and vertical diffusivity K_z in 3 sublayers for all profiles with a SCML. The water columns have been segmented into three sublayers: the layer above the SCML (a,b,c,d), the layer containing the SCML (e,f,g,h) and the layer below the SCML (i,j,k,l). Critical values, such R_i = ¼ and Re_b = 15 and 100, have been marked with vertical dashed lines.

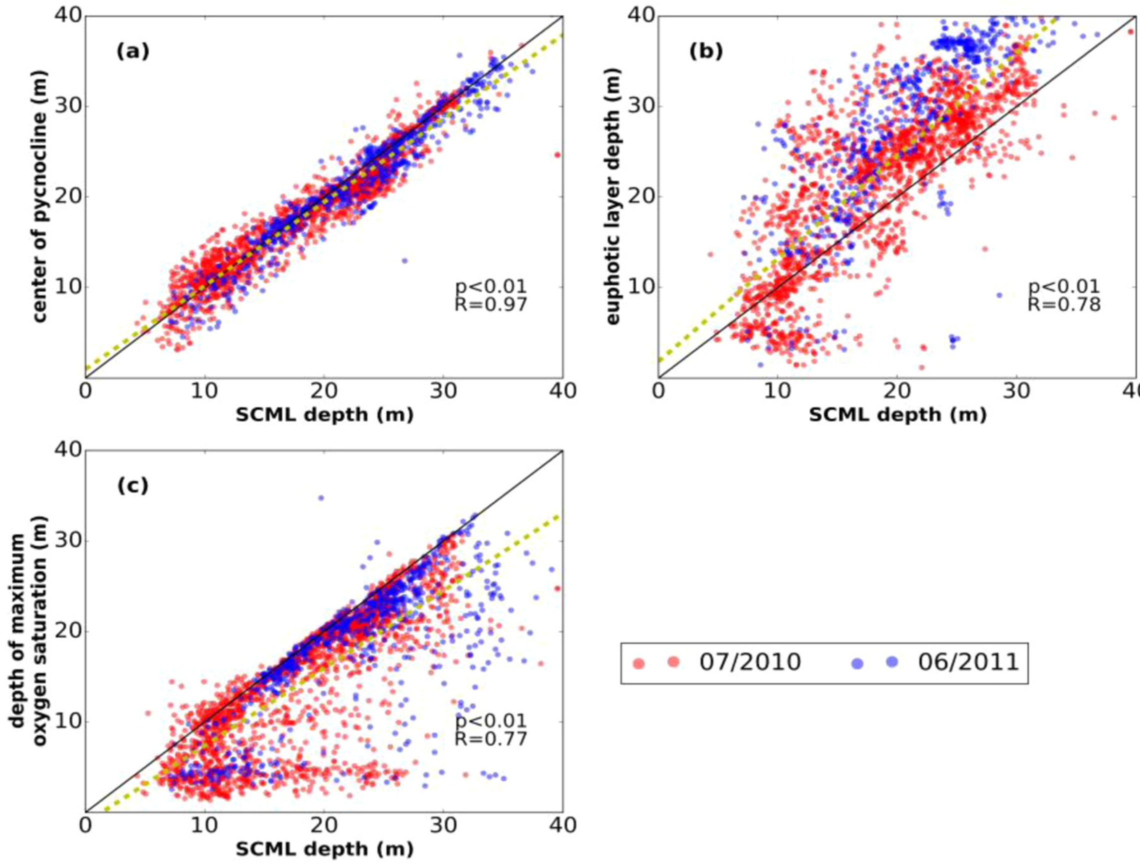

Fig. 6. Pairwise comparison between the depths of the peaks of subsurface CHL maximum layers and the centers of pycnoclines (a), euphotic layer depths (b) and depths of oxygen saturation maxima (c). The regression results are marked by the yellow dashed line, and the 1:1 line is depicted by the black line.

more than half of the records exhibited Re_b values of $> 15\%$, and 10% exhibited Re_b values of > 100; hence, the lower layers were systematically more turbulent than the pycnocline and the upper mixed layer in most profiles, highlighting the dominant role of tidally induced turbulence in the GB. The distribution of vertical diffusivity in the upper and lower mixed layers spanned 6 orders of magnitude, mostly within the range of 10^{-3}–10^{-2} m^2s^{-1}, approximately 3 orders of magnitude higher than that in the pycnocline. The layers corresponding to SCMLs displayed low diffusivity and stable characteristics (Fig. 5). The buoyancy Reynolds number and eddy diffusivity coefficient are not independent of each other; they both rely on the ratio between the dissipation rates and the squared buoyancy frequency. For a given dissipation rate, the higher the buoyancy frequency is, the more stable the interior layer; thus, a SCML is more easily sustained. This was confirmed by the relationship between SCMLs occurrence and the squared buoyancy frequency values for all profiles (Fig. B.1). SCMLs were not observed in weakly stratified water columns until the N^2 reached 0.02 s^{-2}. The occurrence of SCMLs increased with the maximum buoyancy frequency, approaching approximately 90% when the N^2 approached 0.54 s^{-2}.

In addition to the physical conditions, we compared the vertical locations of SCMLs with the pycnocline center and other biochemical parameters to explore the dependence of SCMLs on environmental factors. The CHL peaks in SCMLs were closely co-located with the center of the pycnocline, which we defined as the location of the highest squared buoyancy frequency (Fig. 6a). The locations of CHL peaks in SCMLs were mostly shallower than the euphotic layer depth and were only weakly correlated with the euphotic layer depth (Fig. 6b). Within the euphotic zone, the potential for active photosynthesis is expected, as confirmed by the high correlation between the vertical locations of SCML peaks and highest oxygen saturation values (Fig. 6c). This correlation proved that the SCMLs identified here were photosynthetically active rather than being merely sinking remains. Photosynthesis in SCMLs has also been observed in the Baltic Sea (Bjornsen et al., 1993; Kononen et al., 1998), which were suggested by the consumption of nutrients instead of oxygen, in such an anoxic environment.

3.3.2. Systematic features of SCMLs in the GB

We find that the occurrence of stable SCMLs was related to strong stratification, which reduces turbulent mixing. However, based on previous studies on the preservation of vertical CHL distribution under variable turbulent conditions, several additional mechanisms have been discussed. As suggested by Omand and Mahadevan (2015), the nitracline is co-located with the pycnocline and provides stable conditions with a potentially optimal balance between light and nutrient resources, thereby offering suitable conditions for phytoplankton growth and accumulation (Beckmann and Hense, 2007). In addition, observations have shown that mobile phytoplankton species can swim directionally to nutrient resources diurnally (Cullen and Horrigan, 1981) or position themselves at the nitracline, which can be well below the surface mixed layer depth (Brown et al., 2015). Whether the self-positioning capability of mobile species can result in CHL accumulation depends on how turbulent the physical background setting is compared to the positioning capability of the phytoplankton. Previous studies evaluated the swimming capability of phytoplankton with respect to turbulent mixing via the Péclet number (Simpson and Sharples, 2012):

$$P_e = \frac{L_s^2/K_z}{L_s/\nu_c} \tag{6}$$

where L_s is a representative length scale, such as the thickness of mixed layers or the pycnocline, K_z is the vertical diffusivity, and ν_c is the vertical swimming speed of phytoplankton.

The Péclet number indicates that turbulent diffusion dominates over motility for $P_e < < 1$, while phytoplankton have appreciable control over their position when $P_e > > 1$. If we consider K_z to $10^{-2.5} m^2 \bullet s^{-1}$ for the mixed layer and assume that the length of the mixed layer depth is 15 m for the GB, with typical swimming speeds of phytoplankton ν_c on the order of 10^{-4} m s^{-1} (Cullen and Horrigan, 1981), the Péclet number would correspond to a value of 0.47, which implies that mobile phytoplankton cells would have difficulty positioning themselves in the mixed layer. Once phytoplankton cells are mixed into the vicinity of the pycnocline where K_z is assumed to be $10^{-5} m^2 \bullet s^{-1}$ and the presumably extent is approximately 6 m, the Péclet number would reach 60, indicating that a vertical position in the pycnocline could by maintained by mobile phytoplankton. If we consider that the swimming speed varies among species and when taking typically species in GB in summer, such as species of the genera *Ceratium* and *Dinophysis* (Löder et al., 2012), given the typical swimming speed as 250 $\mu m s^{-1}$ (Levandowsky and Kaneta, 1987) and 104 $\mu m s^{-1}$ (Nielsen and Kiørboe, 2015), the result holds.

In areas with seasonal stable stratification, the CHL concentration has been previously related to physical factors. For example, the CHL concentration decreases with depth (Brown et al., 2015) or increases after nutrients are entrained by wind-driven mixing events (Carranza and Gille, 2014). Based on our data, there were no obvious instantaneous correlations between the vertical CHL distribution and other physical or biological factors, except that the spatial pattern of integrated CHL concentrations in the euphotic zone, i.e. their local maxima, were associated with the occurrence of fronts (not shown here). Time lag correlations could not be studied based on only the snapshots from the SCANFISH data. Our data are not suitable to resolve the revolution process of stratification and the development of SCML, especially in such a shallow and energetic system as the GB, where stratification can be interrupted by strong wind induced mixing, even in summer. In contrast to the southern North Sea, the deeper northern North Sea possesses more stable stratification in summer. The SCMLs in the northern Dogger Bank area have been confirmed to have long durations and to be highly consistent based on observations and simulations (Fernand et al., 2013).

The representativeness of our SCANFISH sampling data for the physical and biological characteristics in the GB merits attention. Considering that the weather condition is representative in the specific years and locations but not necessarily represent the climatological conditions in longer time scales (Geyer et al., 2015), we expected that, the GB should be more turbulent and less stratified than the conditions revealed by our data sets. If continuous data sets covering longer time scales are available, profiles with SCMLs are likely to account for lower proportions.

3.3.3. SCML dynamics during wind mixing

Complementary to the deduction from the statistical analysis, the vertical CHL distribution pattern associated with the hydrodynamic environment has been discussed in a case study. Two transects were sampled twice in July 2010 during campaign 331, i.e., on July 14th and 16th, before and after a significant wind event. The western branch transect extended from 54.2ºN to 55.0ºN in the longitudinal direction, and the northern branch transect extended from 6.3ºE to 7.5ºE in the latitudinal direction (Fig. 1). Since wind mixing events triggered by wind, as pointed out by former studies (Rumyantseva et al., 2015; Williams et al., 2013), are able to re-erode SCM in pycnocline and supply nitrate into pycnocline or even reach the surface water column. We used these sections to explore the conditions under which SCMLs persist or decay during a wind mixing event and how the vertical CHL distribution evolves with changes in the hydrodynamic setting.

According to the re-analysis product from the NCEP Climate Forecast System (Saha et al., 2010), the weather conditions were mild before and during the first sampling event. The wind speed did not exceed 5.38 m s^{-1} during the 24 h before the sampling began (July 13th, 4:00) or during the sampling. In the early morning of July 15th, wind speeds increased and reached 13.77 m s^{-1} at 13:00 on July 15th and dropped to 7.7 m s^{-1} at 16:00 on July 16th. From the early morning of the 15th until noon on the 16th, more than half of the hourly averaged wind speed values were greater than 12 m s^{-1}. The second sampling of the western branch was performed during the diminishing phases of the wind event. For the northern branch, the second sampling was performed after the wind event, when the wind speed was comparable to the earlier calm conditions.

On July 14th before the storm, stable stratification was observed in both transects. A double-pycnocline structure (Fig. 7) was present and contained an intermediary zone with CHL concentrations that were higher than those in the upper mixed layer. A well-structured SCML was present at the base of the lower pycnocline, with average values of 8.1 a.u. in the western branch (Fig. 7a) and 10.0 a.u. in the northern branch (Fig. 7e). In the western branch, below the second pycnocline, the lower mixed layer showed an average CHL concentration of 4.8 a.u., which was around 5 times higher than that in the surface mixed layer (Fig. 7a). Compared to the western branch, there was no evidence for resuspension in the northern branch, and the CHL concentration in the lower mixed layer was comparable to that in the upper mixed layer (Fig. 7e). At the eastern end of the northern transect, the water depth is less than 20 m. Here, CHL concentrations are enhanced in the surface mixed layer, even if a high subsurface CHL concentrations are detectable (Fig. 7e).

Based on a comparison of the observations before and after the storm event, the upper pycnocline vanished as a result of wind-driven mixing, but the lower pycnocline persisted in most areas. In the western branch, the SCML at the base of the lower pycnocline in the first sampling event disappeared (Fig. 7b), except in areas between 54.4°N and 54.5°N where the subsurface CHL layer was more visible than before. Resuspension was prominent in the middle part of the western branch. At the southern end (54.2–54.4°N) of the western branch, the pycnocline broke down, and the CHL subsurface layer decayed (Fig. 7b). In the northern branch, most of the subsurface CHL layer persisted except at the eastern end, where both the pycnocline and the subsurface CHL layer were absent in the second sampling (Fig. 7f).

The persistence or decay of the pycnocline and the corresponding spatial variability was in line with the stability of stratification as quantified by the Simpson-Hunter number (Fig. 7d, h). A higher Simpson-Hunter number indicates stronger tidal mixing, making the stratification more susceptible to mixing. The decay of the pycnocline demonstrated the sensitivity of the stratification to wind events in the shallow southern North Sea, which has been illustrated in previous studies involving simulations (Schrum et al., 2003a, 2003b; Schrum, 1997) and observations (Carpenter et al., 2016; Schultze et al., 2017).

The spatial persistence and decay of the stratification was basically in line with hydrodynamic characteristics, whereas the variation of SCMLs was more complex. Most SCMLs decayed during this wind event. Because of the weakening of the double pycnocline structure after the wind event, the upper boundary of the whole stratified interior (including the whole double pycnocline structure in the first sampling) deepened by approximately 10 m. Furthermore, considering that the SCML was located at the base of the lower pycnocline, we compared the upper and lower boundaries of the lower pycnocline in the first sampling to those in the second sampling. The upper boundary of the lower pycnocline deepened after the wind event in most parts of the two branches (Fig. 7c, g). The variation in the lower boundary of the stratified layer fluctuated around 0, but remained mainly positive, indicating that most of the lower boundary deepened. It is likely that the accumulated CHL was mixed up during the deepening of the pycnocline. Although, it cannot entirely be excluded that biological processes which could contribute to the changes, it is rather unlikely because these are usually not effective enough on such short time scales. The variation in CHL concentration throughout the whole water column and

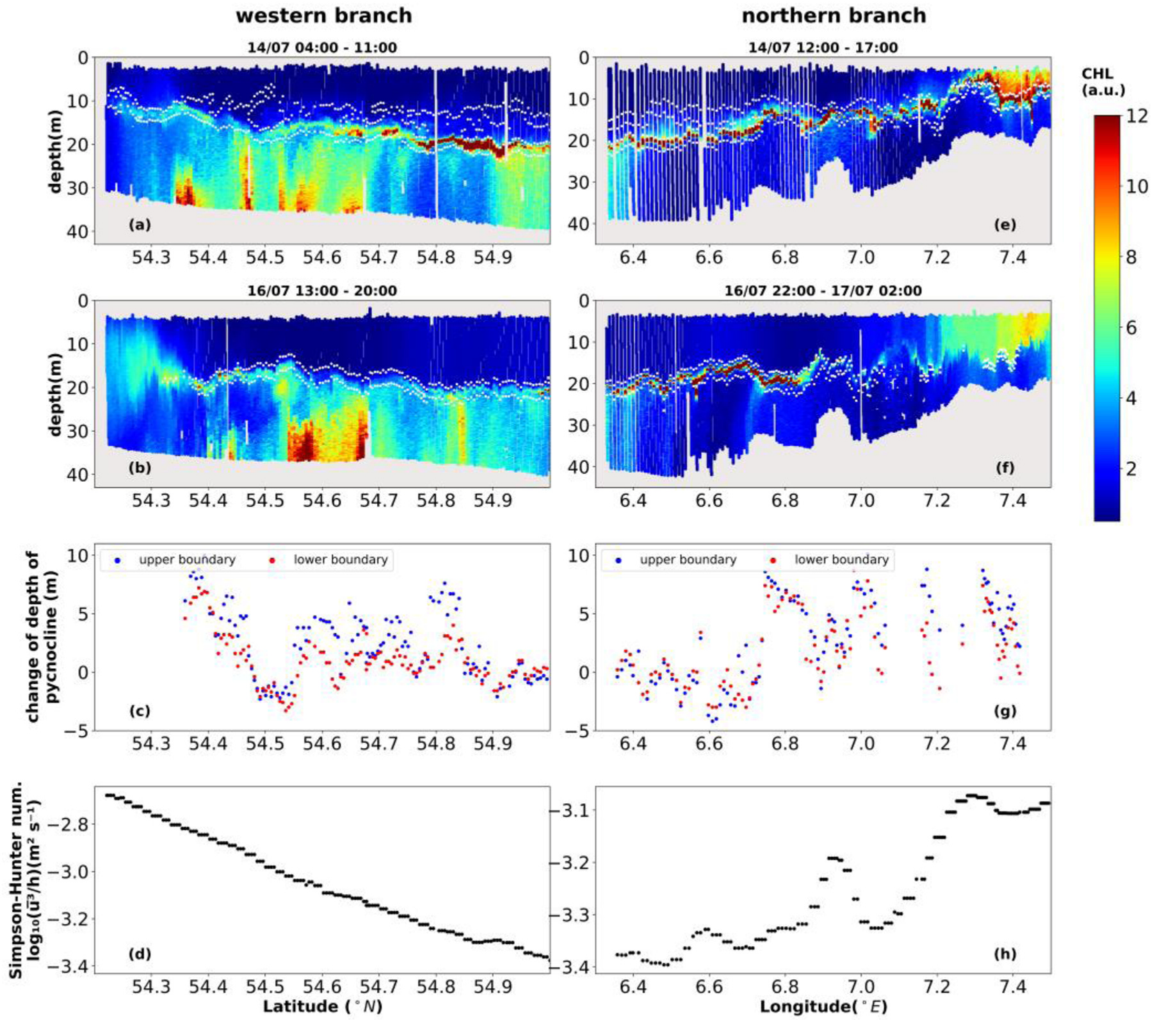

Fig. 7. Scatter plot of CHL (arbitrary units) of two transects measured on 14/07/2010 and repeated on 16/07/2010. The western branch is plotted in the left panels (a,b), and the northern branch is plotted in the right panels (e,f). The detected pycnocline is depicted by white dots for reference. The variations in the depths of the upper and lower boundaries of the pycnocline are depicted in (c) and (g). The distributions of the Simpson-Hunter number are shown in (d) and (h).

in each sublayer divided by the pycnocline was in the range of the natural growth of phytoplankton, but again, natural growth in low light conditions would be an unlikely candidate for the changes. The increase in CHL concentration in the lower mixed layer in the western branch could also come from resuspension (Fig. 7b). The increase in CHL concentration in the upper mixed layer could be either mixed up from a pre-existing SCML or produced following the entrainment of nutrients from lower layers due to the deepening of the pycnocline. The decrease in CHL concentration in the stratified interior could also be induced by enhanced grazing due to suspended zooplankton during wind events, but again this can be considered as rather unlikely due to short time-scale and substantial turbulence during the wind event, which would limit capturing success of zooplankton.

3.4. The formation of high CHL concentrations in the lower layers (HCL)

The HCL-type profiles occur frequently, especially in campaigns performed in late spring (Fig. 4). Thus, an exploration of the mechanisms leading to high CHL in the bottom mixed layer is necessary. It is possible that this phenomenon results from different directions of residual currents below and above the pycnocline, which bring phytoplankton from different source regions to the same area (McCandliss et al., 2002). This might be the case especially for floating and non-sinking species, such as *phaeosystis* which also dominates in the German Bight in spring (Iriarte et al., 1991) (together with diatoms). If the local vertical mixing plays a role, there are two related hypotheses: 1) the HCL type profiles involves CHL from layers above either because of sinking or erosion from pre-existing SCMLs or 2) the HCL type involves CHL from below because of re-suspension effects. In this section, we first test these two hypotheses by investigating CHL gradients near the bottom and in the lower layers of water columns. Afterwards, potential hydrodynamic drivers and responsible biochemical factors will be discussed.

Resuspension has been quantified by the presence of a CHL peak in the bottom layer (CPB) and a corresponding CHL gradient in the upper boundary of the CPB. Among the HCL profiles, 30% had detectable CPBs, whereas only 5.7% of SCM profiles and 15% of SCM-HCL profiles had CPBs. The relative upward gradients in the CPBs in HCL profiles were generally larger than those of SCM and SCM-HCL profiles. The higher occurrence of resuspension signals and higher gradients in the upper branch of the CPBs indicate the importance of resuspension in the formation of HCL-type profiles. In addition to the CPB, the CHL gradients in the lower layer (CGL) can be used to approximate the CHL variation with depth across a relatively long vertical segment. In all profiles classified as SCM, CHL continually decreased from the base of the SCML to the bottom. Furthermore, 76% of SCM-HCL profiles also showed higher CHL concentrations at the base of the SCML, indicating that CHL was mixed down or sank from the subsurface layers. However,

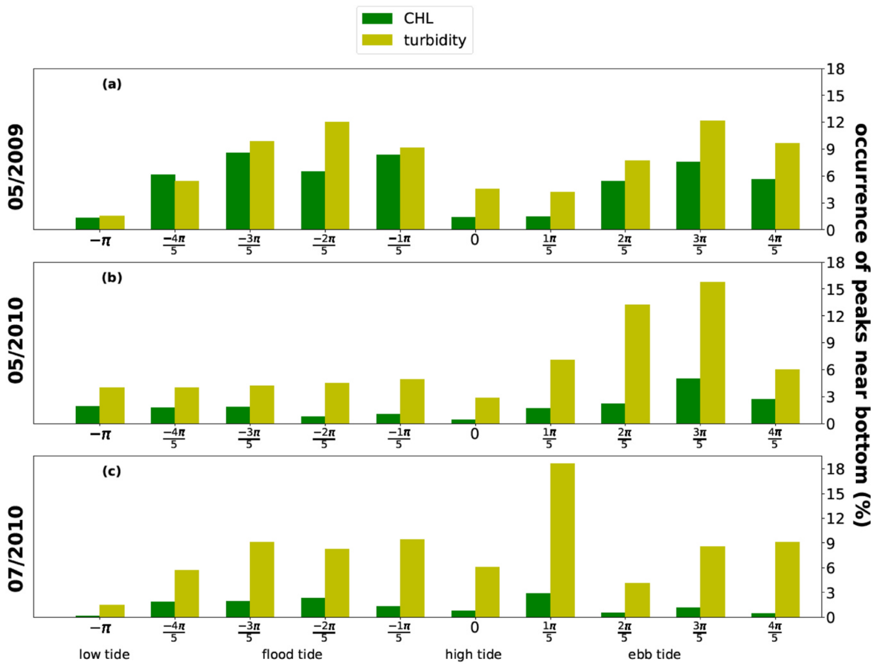

Fig. 8. The occurrence of CHL peaks near the bottom (CPBs) with respect to the tidal cycle. The number of profiles with recognized CPBs was divided by the number of profiles sampled in the corresponding tidal phase interval, yielding the occurrence shown here. Labels on the X-axis represent the tidal cycle: Pi represent low tide; 0 represents high tide; negative values indicate flood tide; positive values indicate ebb tide.

in the remaining 24% of SCM-HCL profiles, the CHL concentration showed that more CHL accumulated towards the bottom. The CHL concentration increased with depth in the lower layers in almost all HCL profiles. By examining the CHL gradients in the bottom mixed layer and the existence of CPBs, we infer that a considerable proportion of the high CHL concentrations come from the bottom in HCL profiles and some SCM-HCL profiles, probably caused by resuspension.

To address the relevance of tides, the dominant hydrodynamic feature in this study area (Otto et al., 1990), to resuspension in the observed profiles, herein we explore the occurrence of resuspension with respect to the tidal cycle, which was retrieved from model simulations. To improve the statistical significance, only campaigns with more than 400 CPBs in total and more than 10 CPBs in each tidal phase segment were included (Fig. 8). We also identified resuspension signals in terms of turbidity as a supplemental forcing indicator, assuming that the resuspension of other materials would not be resource limited, unlike that of CHL.

In the two campaigns performed after the spring bloom, CPBs occurred more frequently during the flood and ebb tidal phases (between $-\frac{3\pi}{5}\sim-\frac{2\pi}{5}$ and $\frac{2\pi}{5}\sim\frac{3\pi}{5}$). Especially in May 2009, the occurrence of CPB during tidal phases $-\frac{4\pi}{5}\sim-\frac{\pi}{5}$and $\frac{\pi}{5}\sim\frac{4\pi}{5}$ was significantly higher than that near the high tidal phases (phase segments around 0) and low tidal phases (phase segments around π) (Fig. 8a). In May 2010, resuspension was only pronounced during ebb time ($\frac{2\pi}{5}\sim\frac{3\pi}{5}$), as was the resuspension based on turbidity signals (Fig. 8b). In contrast, in the campaign performed during the summer, July 2010, the occurrence of resuspension-related CHL signals exhibited no obvious occurrence pattern with the tidal phase (Fig. 8c). Since the occurrence of resuspension-related turbidity signals displayed a better relationship with the tidal cycle, the decoupling between the resuspension of CHL and turbidity in summer indicated the depletion of CHL containing materials.

Resuspension CPB signals only accounted for approximately 10% of the analyzed downward profiles. Even if the criterion of upward gradient of potential CPB was ignored, i.e. resuspension would be considered if profiles with CHL concentration of the peaks near bottom notably higher than the mean CHL concentration in the lower mixed layer, the occurrence of resuspension would not exceed 27% of all analyzed profiles. One reason could be that resuspended CHL is mixed up by strong turbulence. The widespread high CHL concentrations in the lower mixed layer (in HCL and SCM-HCL profiles), for which most profiles showed a smooth curve rather than a steep gradient in the lower layer, could be resulting from the transformation of profiles with significant resuspension signals in the bottom and by further mixing or advection. The efficiency of vertical dispersion can be estimated by the length scale analysis applied by Denman and Gargett (1983):

$$Z(t)^2 = 2K_z t. \tag{7}$$

Given the eddy diffusivity K_z value of $10^{-2.5}$ $m^2 s^{-1}$ in the bottom mixed layer in the GB, it would take 105 min (t) for a cell to be mixed 20 m (Z(t)) vertically away from its original position. Although the vertical diffusivity values are far from vertically homogeneous in the bottom mixed layer, this scale analysis suggests that once CHL-bearing materials on the bottom are resuspended, it would take a short time for them to become mixed throughout the whole lower mixed layer. Bounded by the pycnocline (or an interior layer with low diffusivity), the resuspended CHL would be kept in the lower part of the water column instead of being mixed further upward. Due to the strong tidal mixing in the lower mixed layer, the transient type (SCM-HCL), which only accounts for a small proportion of the measured profiles, should be short-lived. Furthermore, no matter how efficient the bottom tidal currents are in resuspending materials, the resuspension of CHL would be rarely detectable if there is no available resource (Jago and Jones, 1998) at the bottom due to earlier resuspension and/or benthic predation and remineralization.

The seasonal difference in the significance of resuspension signals in CHL profiles could be attributed to seasonal changes of availability of CHL at the bottom. Instead of only using the occurrence of CPBs, which occur in only a small subset of the profiles, we calculated the CHL gradient in the deepest 5 m (CG5) in all the profiles and summarized the increases or decreases in CHL with depth (Fig. 9). The occurrence of positive CG5s, which indicated more CHL available near the bottom than in the adjacent layer above, showed a distinct seasonal pattern. The CG5% increased from approximately 50% in early spring to more than 75% in late spring during the decay of the spring bloom. Thereafter, the percentage decreased throughout summer (30%) to autumn (approximately 20%).

The CG5 seasonality indicated that the resuspension processes of CHL were resource limited in summer and autumn. This pattern was also revealed in the seasonality of vertical CHL distribution patterns (Fig. 4): the proportion of HCL type decreased in summer and especially

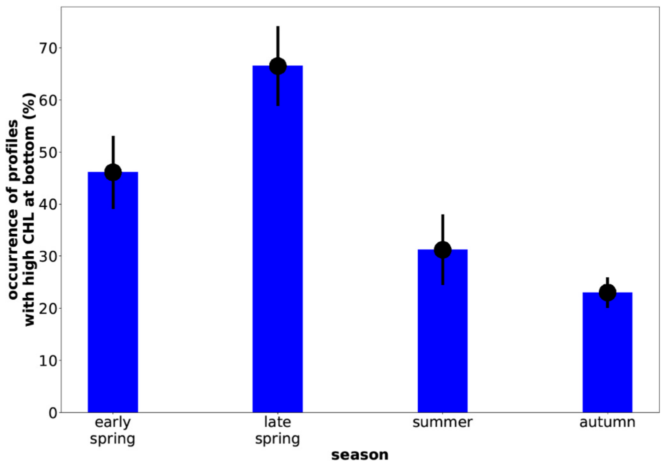

Fig. 9. Percentage of positive CG5 (CHL gradients in the deepest 5 m of profiles) for different seasons. Error bars represent standard deviation among campaigns.

in autumn, when near-bed CHL had been depleted. This seasonal pattern in the availability of resuspension resources at the bottom revealed in our study is similar to previous results for benthic fluff layers. Formed by the sinking of phytoplankton cells, fluff can easily be resuspended and transported (Jago et al., 2002). The amount of fluff resources is greatest after the spring bloom and decreases in other seasons due to resuspension and predation, leading to resource limitation with respect to further resuspension (Jago and Jones, 1998). We have to stay cautious when we derive CHL from fluorescence signal which showed high values near bottom, since fluorescence signals could be influenced by the presence of other organic particles near the bottom, especially in areas with high turbidity, such as the GB. However, the high CHL signals observed near the bottom confirm former measurements of high CHL near bottom at the German Bight and in nearby areas close to the European continent. In these studies, CHL data were derived from water sample directly (Jago and Jones, 1998), from calibrated fluorometer (Millward et al., 1998) or Reineck's box-corer (Dauwe et al., 1998; Jenness and Duineveld, 1985) taken from sea bed. They all confirmed that high CHL concentration can be detected below the pycnocline after the onset of stratification due to phytoplankton sinking or trapped by the pycnoline (Jones et al., 1998). The high concentrations are mostly detectable in late spring because produced organic matters in spring bloom settled down (Boon and Duineveld, 1996; Jago et al., 1993). Compared to other stations (Fourteens, Frisian Front and Skagerrak), the GB showed the strongest predominance of surface deposition and strongest surface accumulation of organic matter at the sea floor, mainly due to longer residence time of water in the GB and the intense local production (Dauwe et al., 1998). Given sufficient settled materials, resuspension driven by tide and waves is detectable (Jago et al., 1993; McCandliss et al., 2002). Due to sinking and aggregation with suspended particulate matter (SPM), the CHL-rich materials in the bottom mixed layer form fluff layers which are also sensitive to resuspension given strong bottom shear stress and sink down in low energy conditions (Jenness and Duineveld, 1985; McCandliss et al., 2002). It is likely that production is able to persist given enough irradiance penetration below the pycnoline (Peeters et al., 1995). However, light limitation plays an important role in controlling primary production in the shallow North Sea, typically in spring and in windy conditions in summer and autumn (Su et al., 2015), since light penetration is very sensitive to resuspension events (Jones et al., 1998).

Separating the resuspension process from sinking based on our data is challenging. It would be problematic to categorize all positive CHL gradients in the bottom mixed layer (increasing CHL concentrations with water depth) as a resuspension signal since many phytoplankton species have a higher densities than water and tend to sink (Smayda, 1971). Especially in the decaying process of the spring bloom, after the nutrients in the surface layer are exhausted, massive amounts of phytoplankton cells sink down. However, the sinking speed of some cells slows once the nutrient status improves and the buoyancy of the cells increases (Steele and Yentsch, 1960). Additionally, some cells may also become neutrally buoyant because of the increasing density with depth.

In addition to CHL accumulating near the bottom, high CHL concentrations in the lower layers may also come from overlying SCMLs, as 76% of SCM-HCLs displayed higher CHL concentrations at the base of the pycnocline than that of segments further below. Considering physical processes, removal of CHL from a pre-existing SCML can result in high CHL concentration at the base of the pycnocline (Sharples et al., 2001). If the elevated CHL levels in the pycnocline are eroded by tidal currents, periodic downward pulses of biomass should be resolved in the time series. This hypothesis has already been corroborated in simulations of frontal systems in which periodic mixing/stratifying processes and the consequent biomass distribution were shown (Schrum et al., 2006; Sharples, 2008). When the turbulent mixing energy in the lower layer reaches the pycnocline, the high gradient of CHL at the base of a SCML can be smoothed or the whole SCM structure can be eroded. A SCM profile can be transformed into an HCL-SCM profile or even an HCL profile when the subsurface layer structure is eroded and disappeared. This assumption was further supported by comparable vertically integrated CHL concentration in the water segment including pycnocline and lower mixed layer in different CHL vertical distribution types (SCM-HCL, HCL, SCM), under conditions that these different CHL vertical distribution type profiles were detected in adjacent areas (Table B1). Notably, tidal mixing processes from the bottom are not always detrimental to the persistence of SCMLs. In addition to mixing organic matter from an SCML down to the bottom of the water column, tidal mixing can also inject nutrients into the pycnocline, triggering the production and maintenance of photosynthetic activity there (Sharples et al., 2007; Zhao et al., 2018). The vertical mixing rates can also influence the persistence of sinking species in the bottom mixed layer by returning phytoplankton cells to depths where irradiance is high enough to sustain photosynthetic activity (Huisman et al., 2002). The light availability is also sensitive to the existence of SCMLs but also to increasing turbidity by mixing.

In the GB system, most SCMLs are shallower than the euphotic layer depth (Fig. 6b), which also indicates that high CHL below the pycnocline has the chance to stay photosynthetic active. This mechanism can further support the formation of HCL and SCM-HCL. This is an interpretation besides the vertical mixing mechanism since phytoplankton biomass or CHL are not conservative. Light penetration below the pycnoline has higher occurrence in summer when the self-shading is not as strong as in spring (Table 2)

Limited by the data availability (no nutrient data and no particulate organic carbon data), we do not have the chance to further investigate biological factors in the vertical CHL distribution. Moreover, the measured CHL concentrations can not be converted directly to biomass and

Table 2
Occurrence of profiles with euphotic layer depth deeper than the lower limit of pycnocline.

Campaign	HCL type profile Eup. deeper than pyc.(%)	SCM-HCL type profile Eup. deeper than pyc.(%)
07/2010	85.4	81.6
06/2011	74.6	85.7
05/2010	48.1	/
05/2009	8.98	/
08/2009	70.9	16.7
09/2009	50.0	/
03/2010	/	/
09/2010	/	/
04/2011	84.0	/
09/2011	/	/

quantitative estimates are hardly possible, since the CHL:C ratio is variable among species and sensitive to the environment and season, particularly in coastal areas (Alvarez-Fernandez and Riegman, 2014). Given adequate nutrients and low irradiance levels, which meet the lower threshold for sustaining photosynthetic activity, phytoplankton cells tend to use nutrients to generate more pigments to harvest more light energy instead of building biomass (Geider et al., 1997; Macintyre et al., 2000). In reality, the measured CHL-rich patches may consist of multiple species with different light and nutrient requirements. More nutrient-efficient competitors should dominate the upper part of the SCML, whereas superior light competitors should mainly inhabit the lower part of the SCML (Huisman et al., 2004). Oscillations in physical mixing, which modify the dispersion rates of phytoplankton and the upward flux of nutrients, could further promote the phytoplankton diversity (Huisman et al., 2006). Implementing a variable allocation of internal resources, simulations suggest that the vertical CHL distribution in the GB critically depends on the cellular storage of nutrients and pigmentary materials (Kerimoglu et al., 2017).

4. Conclusions

By performing an in-depth analysis of vertical CHL profiles in the inner German Bight (GB), we studied the heterogeneity in vertical CHL distribution using measured high-resolution vertical transects. Our analysis provided the first quantitative description on heterogeneity & homogeneity of vertical CHL distribution in the GB and explores potential mechanisms. More than half of profiles show vertical homogeneous distribution of CHL; extrapolating this to the full range of weather conditions, this proportion would further increase considering that the averaged hydrodynamic background is more turbulent than in our observations which mainly encountered calm whether conditions. However, heterogeneous vertical distribution of CHL, especially in stratified season, merits more attention. After the onset of stratification in late spring, higher CHL in the bottom mixed layer than that in the surface layer has been observed. Several mechanisms may lead to this phenomenon, such as diatoms' sinking, water mass advection and phyto-acclimation. Due to the shallowness of the GB, in more than half of the profiles with high CHL concentration below the pycnocline, the euphotic layer depth is deeper than the lower limit of the pycnocline, which indicates that phytoplankton cells in the lower layer have the chance to access enough irradiance to keep photosynthesis active. However, the frequently observed high bottom concentrations can hardly be explained by local growth; resuspension was identified as an important candidate to explain this phenomen.

Our study revealed that the vertical distribution of CHL in a shallow and tidally energetic system can be attribute to both physical processes (i.e. resuspension and turbulent mixing) and biological processes (i.e. growth and sinking of phytoplankton cells). The large fraction of near-bottom high CHL regimes in the stratified season indicates the importance of the benthic-pelagic coupling in tidally energetic shallow areas, such as the German Bight and points to the importance to consider this adequately in theory and modelling studies in tidally influenced shallow seas, which has implications for estimates of carbon flux (Bauer et al., 2013) and nutrients cycling (Beckmann and Hense, 2017). In such a shallow area where small proportion of organic matters will be mineralized in the water column (Lutz et al., 2002; Suess, 1980), the interface of water column and sediments acts as buffer to release nutrients slowly long after the most productive season (Provoost et al., 2013). Particularly in the southern North Sea, the resuspension process (Thompson et al., 2011), the activity of macrobenthos and bacteria (Franco et al., 2010) further complicate the benthic-pelagic coupling (Zhang and Wirtz, 2017). Our study and high resolution observations like those presented here, can help to assess model tools and identify structural limitations. For example, a validation of some new ecosystem models using vertical transects of CHL shows that even ecosystem models specifically developed for shallow seas, which reproduce well SCM type profiles might have difficulties to do so for the HCL type (Baschek et al., 2017; Kerimoglu et al., 2017). This points to the need to improve process descriptions and parametrizations in modelling tools for coastal areas.

Moreover, since seasonality modulates the vertical heterogeneity of CHL distribution, our study suggests refined in-situ monitoring, with more vertical sampling required in deeper areas during the stratified season (Fernand et al., 2013). Besides, our study points also to the need to develop new approaches to conclude on productivity from remote sensing for stratified shallow shelf sea, since subsurface CHL maxima in those regions may provide a reasonable source of error for remote sensing based estimates (Stramska and Stramski, 2005; Yacobi, 2006). We drew conclusions in this study mainly based on statistical analysis. To analyze the vertical distribution of CHL in a simultaneous bio-physical way, coinciding measurements of vertical CHL profile, organic matter and physical settings are necessary (Ediger et al., 2005; Liu et al., 2017; Sharples et al., 2007). For example, adding observations of particulate organic carbon and CHL data sampled by HPLC method in future studies will provide reliable data sets to investigate physiological contributions to the CHL profiles and evaluate the exchange of organic matter between the upper layer and the bottom layer (McTigue et al., 2015; Smith et al., 2012).

Acknowledgments

The first author would like to express her gratitude to the financial support from the China Scholarship Council (CSC. No.: 201406140121). All authors are indebted to the masters and crews of the research vessel RV Heincke and the different chief scientist conducting the cruises. The cruises were conducted under the grant numbers: AWI-HE303-00, AWI-HE308-00, AWI-HE312-00, AWI-HE319-00, AWI-HE325-00, AWI-HE331-00, AWI-HE336-00, AWI-HE353-00, AWI-HE359-00, AWI-HE365-00. All authors thank H. Rink, H. Thomas, M. Heineke, and R. Kopetzky, for operating the SCANFISH, for processing and quality assurance of the observational data and laboratory work. We are grateful to Kerstin Heymann for performing the HPLC analysis. We thank Ryan North, Ingrid M. Angel-Benavides, Lucas Merckelbach, Jeffrey Carpenter and Yangyang Liu for their suggestions regarding data processing. The GETM simulation data were provided by Ulf Gräwe and Onur Kerimoglu. Use of the remote sensing data was suggested by Hajo Krasemann.

Appendix A. Data calibration and adjustment, method uncertainty and classification details

During these campaigns, samples for chlorophyll a measured by HPLC were collected simultaneously along the SCANFISH transects. At most stations, one sample was taken in the surface layer when the water column is mixed or above the pycnoline when it is stratified. When a stratified water column was encountered, sometimes, a deeper sample was additionally taken below the pycnocline. In total, 124 samples from the surface layer are available; and 59 from subsurface layers. We made use of these data to estimate the general ratio between the CHL concentration and fluorescence signal and to prove that the F: CHL ratio obeys a good linear correlation and does not varied significantly among different season and years. For the classification strategy used for identifying CHL vertical distribution types, we chose a criterion which is significant enough to exceed

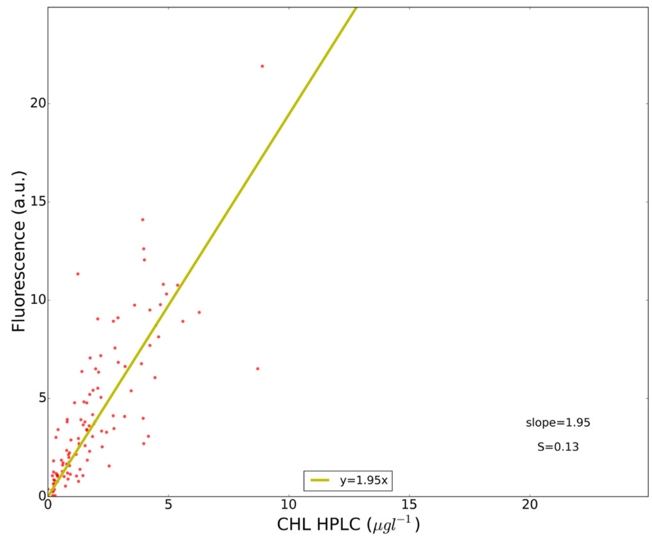

Fig. A1. Relationship between the CHL concentrations estimated from the HPLC measurements and fluorescence value measured by fluorometer.

the range of the uncertainty of F: CHL ratio, therefore the difference of fluorescence over the water column does reflect differences in CHL concentrations, rather than resulting from strongly varying F: CHL ratio. Finally, the classification method was applied for fluorescence profile and HPLC measured CHL data. The similar outcomes from fluorescence profile and HPLC measured CHL data further prove the robustness of the classification method.

The relationship between CHL concentrations and fluorescence was investigated by a simple linear regression analysis. The influence of fluorescence quenching on this relationship was reduced by discarding any data taken around the local noon (9 a.m. to 3 p.m.). For all data points, the obtained regression ratio (F: CHL) is 1.95, with standard error (S) ± 0.13 (with unit of a.u.), from 111 available samples (n) (Fig. A.1). After further distinguishing between below and above pycnocline samples, we found that the F: CHL is 2.15 ± 0.16 in surface samples (n = 76) and 1.73 ± 0.23 in subsurface samples (n = 35) (Table A1). We also checked the F: CHL ratio for its seasonal and inter-annual variability. The F: CHL is 1.95 ± 0.20 in spring (n = 59), 2.28 ± 0.17 in summer (n = 40 and 1.39 ± 0.25 in autumn (n = 12). For different years, the F: CHL is 1.53 ± 0.20 in 2009 (n = 38), 2.10 ± 0.17 in 2010 (n = 49, R = 0.87) and 2.27 ± 0.36 in 2011 (n = 24) (Table A1). Generally, the fluorescence and HPLC measured CHL show a linear relation and the regression is not sensitive to season or inter-annual variability. F: CHL mainly lies in the range between 1.4 and 2.3; the seasonal and inter-annual variability varies but not more than a factor of 2. We take this variation range into consideration when we set the criterion in the classification method (Section 2.3). The influence of varied F: CHL on the classification method was also estimated and given in the following paragraph.

Regarding to the classification of profile types, the issue really matters is the F: CHL's vertical variation within each profile instead of F: CHL's absolute variation among different profiles. To check the relevant influence, we make use of HPLC measured CHL with both surface and subsurface data in the same profile. To quantify the relative variation of F: CHL, we calculated the percentage of profiles with the subsurface vs. surface F: CHL ratio (F: CHL(subsurface/surface)) with value in the range of 0.5–2.0. For dataset excluding noon hours, the percentage is 66.7% (n * = 33) (Fig. A.2). We also checked the seasonal and inter-annual variability (Tabel.A.2). The 0.5 < F: CHL(subsurface/surface) < 2.0% is 61.1% in spring (n * = 18), 71.4% in summer (n = 14). The variation in autumn has not been discussed since there are only 4 profiles available. For the inter-annual variability, the 0.5 < F: CHL(subsurface/surface) < 2.0% is 59.2% in 2009 (n = 13), 66.7% in 2010 (n = 15) and 60% in 2011 (n = 5). As

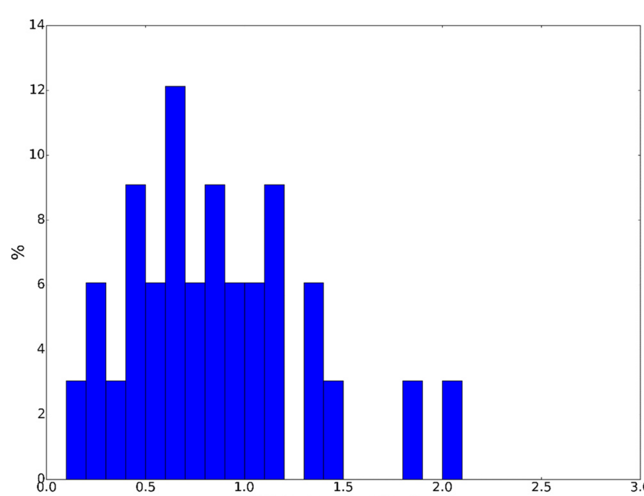

Fig. A.2. Distribution of F:CHL (subsurface/surface) value. Profiles influenced by quenching have been excluded for this analysis.

Table A1
Uncertainty of F: CHL ratio.

Campaign	F: CHL	S	n	0.5 < F: CHL(subsurface/surface) < 2.0 (%)	n*
all samples	1.95(2.0)	0.13(0.13)	111(183)	66.66(56.6)	33(53)
surface	2.15(2.20)	0.16(0.15)	76(124)	/	/
Subsurface	1.73(1.79)	0.23(0.25)	35(59)	/	/
Season	**F: CHL**	**S**	**n**	**0.5 < F: CHL(subsurface/surface) < 2.0 (%)**	**n***
Spring	1.95(2.08)	0.20(0.20)	59(86)	61.1(62.5)	18(24)
Summer	2.28(2.14)	0.17(0.22)	40(71)	71.4(56.0)	14(25)
Autumn	1.39(1.55)	0.25(0.22)	12(26)	100(25.0)	1(4)
Year	**F: CHL**	**S**	**n**	**0.5 < F: CHL(subsurface/surface) < 2 (%)**	**n***
2009	1.53(1.73)	0.20(0.26)	38(67)	69.2(50.0)	13(24)
2010	2.10(2.14)	0.17(0.16)	49(71)	66.7(66.7)	15(21)
2011	2.27(2.31)	0.36(0.25)	24(45)	60.0(50.0)	5(8)

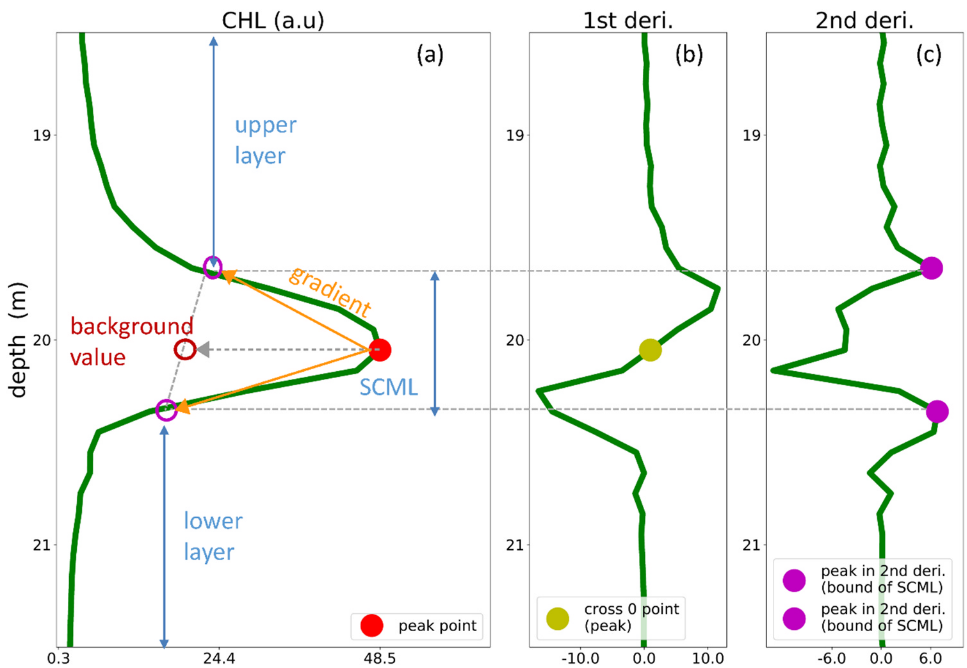

Fig. A3. Schematic diagram for SCML detection in an exemplary CHL profile (a). First (b) and second -order derivative (c) of the measured profiles are used to identify the position of the SCML peak and SCML boundary.

suggested by these cross-validation tests, a factor of 2 in fluorescence between the vertical layers is used as the criterion in the classification of CHL vertical distribution types (Section 2.3). This factor also takes the F: CHL's inter-annual variability and seasonal variability into account.

When we apply the same criterion to classify the fluorescence profile and observed HPLC CHL which possesses both surface and subsurface samples in one station, 75% of joint HPLC CHL samples and fluorescence profiles coming from the same station provide the same profile classification. This is a rather high agreement in classification, taking into account factors adding uncertainty such as comparing profile to single point estimates, the influence of quenching and the variation of CHL fluorescence signals in dependence of species, light availability and other conditions.

Only fluorescence values sampled deeper than 30 m can be assumed to be free of quenching (Guinet et al., 2013), which only holds for the deep ocean but not for shallow coastal waters. We therefore adjusted the surface segment of fluorescence vertical profiles, if the profile was sampled at noon (9 a.m. to 3 p.m.). To identify quenching in noon-profiles, we used exponential regression. If the portion of the profile above the pycnocline (in stratified case) or above the shallowest local maximum fits an exponential regression and the amplitude increases with depth, the influence from quenching is confirmed. In case of a mixed water column, the first local maximum is used to replace all values above (Xing et al., 2012). For the stratified water column, the fluorescence value in the upper limit of the pycnocline was used to replace all values above. In some cases, the quenching effect might pass through the mixed layer into the stratified layer and influence the fluorescence shape within and above the pycnocline, which might be the major source of uncertainty. If the value of surface fluorescence profile approached 0 and showed strong fluctuations which

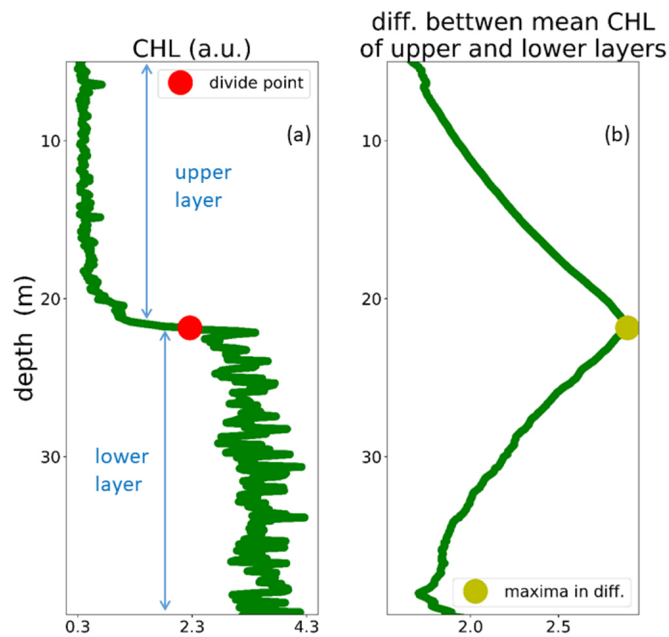

Fig. A4. Schematic diagram for the division of sublayers without a SCML.

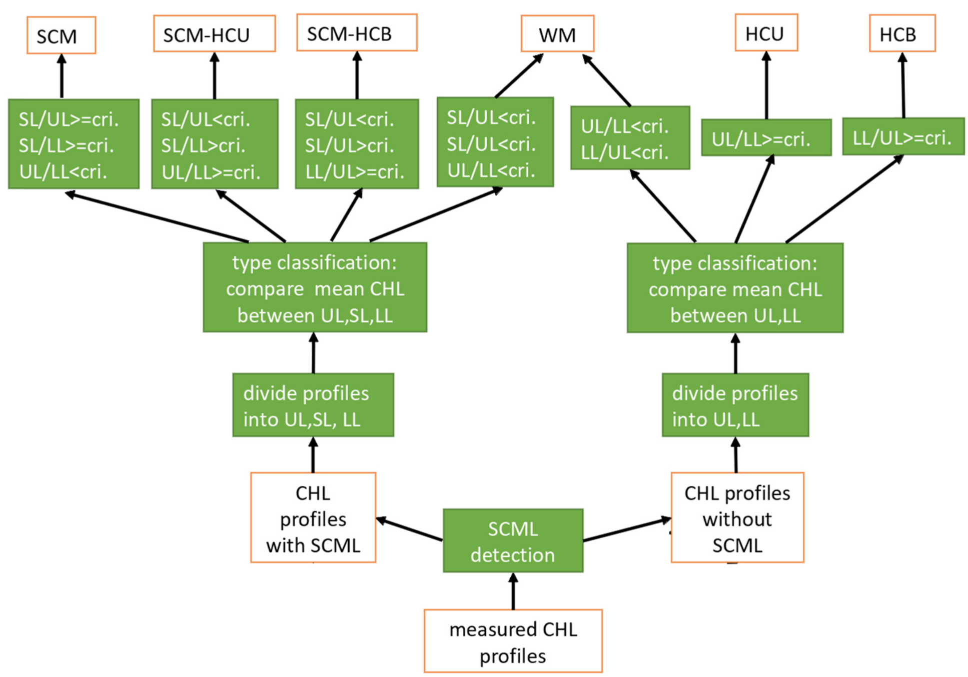

Fig. A5. Flow chart of the classification of CHL profiles.

indicated strong quenching and prohibited exponential fitting, the profile was discarded in following analysis. However, strong quenching rarely happens in the study area.

Appendix B

To test whether vertical mixing could influence vertical distribution of CHL concentration and result in different CHL vertical distribution types (HCL, SCM-HCL, SCM) among adjacent profiles, we compared vertically integrated CHL concentrations in the pycnocline and in lower mixed layers from horizontally adjacent profiles, under the condition that adjacent profiles are classified in different CHL vertical distribution types (HCL, SCM-HCL, SCM) as mentioned above.

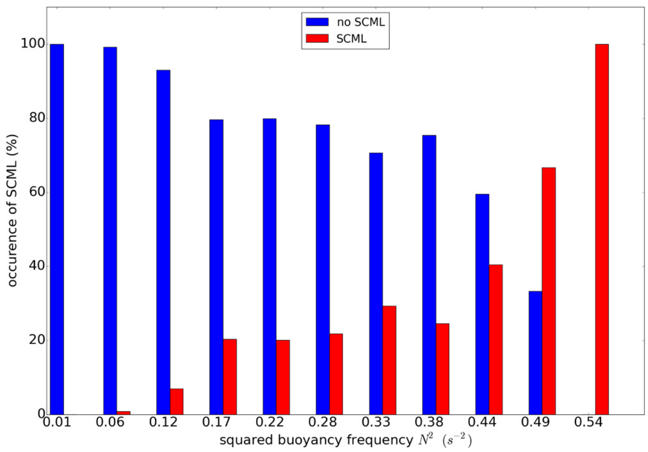

Fig. B.1. The occurrence of subsurface CHL maximum layers in different stratification conditions. The stratification intensity is quantified by the maximum squared buoyancy frequency (N^2) in measured profiles. Note that values of N^2 beyond the listed range are included in the segments of the upper or lower boundaries.

Table B1
relative change of vertical integrated CHL within the pycnocline and bottom mixed layer in different CHL vertical profile types.

Campaign	CHL ratio HCL/SCM (%)	CHL ratio SCM-HCL/SCM (%)	CHL ratio SCM-HCL/HCL (%)
2010,07	70.0	84.3	119.0
2009,08	105.7	115.9	110.0

We pooled profiles classified in type HCL, type SCM-HCL and type SCM within horizontally adjacent 12 profiles (spatial range: 1500–2400 m) and calculated the relative change of integrated CHL concentration in the water column segments including the pycnocline and lower mixed layer. The relative changes of integrated CHL were quantified by the ratio between different CHL vertical distribution types. In Table B1, the relative changes of integrated CHL concentration between HCL type and SCM type profiles are in the first column, between SCM-HCL and SCM type profiles in the second column, between SCM-HCL and HCL type profiles in the third column. Some adjusting profiles in the campaigns July 2010 and August 2009 revealed that relative changes of vertically integrated CHL between different types of CHL profiles vary between 70% and 119%. Vertical integrated CHL concentration (ratios between the pycnocline and lower mixed layer) in different CHL vertical distribution types profiles ending up to similar levels supports the erosion hypothesis that vertical mixing regulates the vertical distribution of phytoplankton. However, this holds for discussion in shorter time scales during which phytoplankton growth and mortality are negligible.

References

Alvarez-Fernandez, S., Riegman, R., 2014. Chlorophyll in North Sea coastal and offshore waters does not reflect long term trends of phytoplankton biomass. J. Sea Res. https://doi.org/10.1016/j.seares.2014.04.005.

Babin, M., Roesler, C.S., Cullen, J.J., 2008. Real-time coastal observing systems for marine ecosystem dynamics and harmful algal blooms: theory, instrumentation and modelling. Oceanogr. Methodol. Ser. https://doi.org/10.1016/j.hal.2010.01.002.2.

Banse, K., 2004. Should we continue to use the 1% light depth convention for estimating the compensation depth of phytoplankton for another 70 years. Limnol. Ocean. Bull. 13, 1–4.

Baschek, B., Schroeder, F., Brix, H., Riethmüller, R., Badewien, T.H., Breitbach, G., Brügge, B., Colijn, F., Doerffer, R., Eschenbach, C., Friedrich, J., Fischer, P., Garthe, S., Horstmann, J., Krasemann, H., Metfies, K., Merckelbach, L., Ohle, N., Petersen, W., Pröfrock, D., Röttgers, R., Schlüter, M., Schulz, J., Schulz-Stellenfleth, J., Stanev, E., Staneva, J., Winter, C., Wirtz, K., Wollschläger, J., Zielinski, O., Ziemer, F., 2017. The coastal observing system for northern and arctic seas (COSYNA). Ocean Sci. https://doi.org/10.5194/os-13-379-2017.

Bauer, J.E., Cai, W.J., Raymond, P.A., Bianchi, T.S., Hopkinson, C.S., Regnier, P.A.G., 2013. The changing carbon cycle of the coastal ocean. Nature. https://doi.org/10.1038/nature12857.

Beckmann, A., Hense, I., 2017. The impact of primary and export production on the formation of the secondary nitrite maximum: a model study. Ecol. Modell. 359, 25–33. https://doi.org/10.1016/J.ECOLMODEL.2017.05.014.

Beckmann, A., Hense, I., 2007. Beneath the surface: characteristics of oceanic ecosystems under weak mixing conditions - a theoretical investigation. Prog. Oceanogr. 75, 771–796. https://doi.org/10.1016/j.pocean.2007.09.002.

Benoit-Bird, K.J., Cowles, T.J., Wingard, C.E., 2009. Edge gradients provide evidence of ecological interactions in planktonic thin layers. Limnol. Oceanogr. 54, 1382–1392. https://doi.org/10.4319/lo.2009.54.4.1382.

Beusekom, J. Van, Brockmann, U., 1999. The importance of sediments in the transformation and turnover of nutrients and organic matter in the Wadden Sea and German Bight. Dtsch. https://doi.org/10.1007/BF02764176.

Bjornsen, P.K., Kaas, H., Kaas, H., Nielsen, T.G., Olesen, M., Richardson, K., 1993. Dynamics of a subsurface phytoplankton maximum in the Skagerrak. Mar. Ecol. Prog. Ser. 95, 279–294. https://doi.org/10.3354/meps095279.

Boon, A.R., Duineveld, G.C.A., 1996. Phytopigments and fatty acids as molecular markers for the. J. Sea Res. 35, 279–291.

Boss, E., Behrenfeld, M., 2010. In situ evaluation of the initiation of the North Atlantic phytoplankton bloom. Geophys. Res. Lett. 37, 1–5. https://doi.org/10.1029/2010GL044174.

Brand, L.E., Guillard, R.R.L., 1981. The effects of continuous light and light intensity on the reproduction rates of twenty-two species of marine phytoplankton. J. Exp. Mar. Biol. Ecol. 50, 119–132. https://doi.org/10.1016/0022-0981(81)90045-9.

Brown, Z.W., Lowry, K.E., Palmer, M.A., van Dijken, G.L., Mills, M.M., Pickart, R.S., Arrigo, K.R., 2015. Characterizing the subsurface chlorophyll a maximum in the Chukchi Sea and Canada Basin. Deep. Res. Part II Top. Stud. Oceanogr. https://doi.org/10.1016/j.dsr2.2015.02.010.

Butterworth, S., 1930. On the theory of filter amplifiers. Exp. Wirel. Wirel. Eng (https://doi.org/citeulike-article-id:5322726).

Carpenter, J., Merckelbach, L., Callies, U., Clark, S., Gaslikova, L., B.B., 2016. A multi-decadal wind-wave hindcast for the North Sea 1949–2014 : coastDat2 11, pp. 1–28. ⟨https://doi.org/10.1594/WDCC/coastDat-2⟩.

Carranza, M.M., Gille, S.T., 2014. Wind forcing, mixed-layer depth and Chl-a response in the Southern Ocean, pp. 22–26.

Charnock, H., Dyer, K.R., Huthnance, J.M., Liss, P.S., Simpson, J.H., Tett, P.B., 1993. Understanding the North Sea system. Philos. Trans. - R. Soc. Lond. A.

Claustre, H., Morel, A., Babin, M., Cailliau, C., Marie, D., Marty, J.-C., Tailliez, D., Vaulot, D., 1999. Variability in particle attenuation and chlorophyll fluorescence in the tropical Pacific: scales, patterns, and biogeochemical implications. J. Geophys. Res. https://doi.org/10.1029/98JC01334.

Cullen, J.J., Horrigan, S.G., 1981. Effects of nitrate on the diurnal vertical migration, carbon to nitrogen ratio, and the photosynthetic capacity of the dinoflagellate Gymnodinium splendens. Mar. Biol. https://doi.org/10.1007/BF00388169.

Czitrom, S.P.R., Budéus, G., Krause, G., 1988. A tidal mixing front in an area influenced by land runoff. Cont. Shelf Res. https://doi.org/10.1016/0278-4343(88)90030-1.

Dauwe, B., Herman, P.M.J., Heip, C.H.R., 1998. Community structure and bioturbation potential of manrofauna at four North Sea station with contrasting food supply. Mar. Ecol. Prog. Ser. 173, 67–83. https://doi.org/10.3354/meps173067.

Dekshenieks, M.M., Donaghay, P.L., Sullivan, J.M., Rines, J.E.B., Osborn, T.R., Twardowski, M.S., 2001. Temporal and spatial occurrence of thin phytoplankton layers in relation to physical processes. Mar. Ecol. Prog. Ser. 223, 61–71. https://doi.org/10.3354/meps223061.
Denman, K.L., Gargett, A.E., 1983. Time and space scales of vertical mixing and advection of phytoplankton in the upper ocean. Limnol. Oceanogr. https://doi.org/10.4319/lo.1983.28.5.0801.
Dietrich, G., 1950. Die natüirlichen Regionen der Nord- und Ostsee auf hydrographischer Grundlage.-Kieler Meeres- forschung. Kiel. Meeres- Forsch. 7, 35–69.
Dippner, J.W., 1993. A frontal-resolving model for the German Bight. Cont. Shelf Res. https://doi.org/10.1016/0278-4343(93)90035-V.
Duineveld, G., Boon, A., 2002. Short-term variations in the fluxes and composition of seston in near-bottom traps in the southern North Sea. Helgol. Mar. Res. 56, 140–148. https://doi.org/10.1007/s10152-001-0091-x.
Ediger, D., Tuğrul, S., Yilmaz, A., 2005. Vertical profiles of particulate organic matter and its relationship with chlorophyll-a in the upper layer of the NE Mediterranean Sea. J. Mar. Syst. https://doi.org/10.1016/j.jmarsys.2004.09.003.
Eisma, D., Kalf, J., 1987. Dispersal, concentration and deposition of suspended matter in the North Sea. J. Geol. Soc. 144, 161–178. https://doi.org/10.1144/gsjgs.144.1.0161.
Fernand, L., Weston, K., Morris, T., Greenwood, N., Brown, J., Jickells, T., 2013. The contribution of the deep chlorophyll maximum to primary production in a seasonally stratified shelf sea, the North Sea. Biogeochemistry 113, 153–166. https://doi.org/10.1007/s10533-013-9831-7.
Franco, M., de, A., Vanaverbeke, J., Van Oevelen, D., Soetaert, K., Costa, M.J., Vincx, M., Moens, T., 2010. Respiration partitioning in contrasting subtidal sediments: seasonality and response to a spring phytoplankton deposition. Mar. Ecol. 31, 276–290. https://doi.org/10.1111/j.1439-0485.2009.00319.x.
Gehlen, M., Malschaert, H., Van Raaphorst, W.R., 1995. Spatial and temporal variability of benthic silica fluxes in the southeastern North Sea. Cont. Shelf Res. 15, 1675–1696. https://doi.org/10.1016/0278-4343(95)00012-P.
Geider, R.J., MacIntyre, H.L., Kana, T.M., 1997. Dynamic model of phytoplankton growth and acclimation: responses of the balanced growth rate and the chlorophyll a: carbon ratio to light, nutrient-limitation and temperature. Mar. Ecol. Prog. Ser. https://doi.org/10.3354/meps148187.
Geyer, B., Weisse, R., Bisling, P., Winterfeldt, J., 2015. Climatology of North Sea wind energy derived from a model hindcast for 1958–2012. J. Wind Eng. Ind. Aerodyn. https://doi.org/10.1016/j.jweia.2015.09.005.
Gräwe, U., Holtermann, P., Klingbeil, K., Burchard, H., 2015. Advantages of vertically adaptive coordinates in numerical models of stratified shelf seas. Ocean Model. https://doi.org/10.1016/j.ocemod.2015.05.008.
Grenander, U., 1959. Probability and Statistics. John Wiley and Sons.
Guinet, C., Xing, X., Walker, E., Monestiez, P., Marchand, S., Picard, B., Jaud, T., Authier, M., Cotté, C., Dragon, A.C., Diamond, E., Antoine, D., Lovell, P., Blain, S., D'Ortenzio, F., Claustre, H., 2013. Calibration procedures and first dataset of Southern Ocean chlorophyll a profiles collected by elephant seals equipped with a newly developed CTD-fluorescence tags. Earth Syst. Sci. Data 5, 15–29. https://doi.org/10.5194/essd-5-15-2013.
Haren H. Van, Howarth M.J., 2004. Enhanced stability during reduction of stratification in the North Sea, 24, pp. 805–819. 〈https://doi.org/10.1016/j.csr.2004.01.008〉.
Herdman, W.A.S., 1923. Noounders of Oceanography and their Work; An Introduction to the Science of the Sea. E. Arnold & Co., London. https://doi.org/10.5962/bhl.title.16362.
Hofmeister, R., Beckers, J.M., Burchard, H., 2011. Realistic modelling of the exceptional inflows into the central Baltic Sea in 2003 using terrain-following coordinates. Ocean Model. https://doi.org/10.1016/j.ocemod.2011.04.007.
Huisman, J., Arraya, M., Ebert, U., Sommeijer, B., 2002. How do sinking phytoplankton species manage to persist ? 159.
Huisman, J., Pham Thi, N.N., Karl, D.M., Sommeijer, B., 2006. Reduced mixing generates oscillations and chaos in the oceanic deep chlorophyll maximum. Nature. https://doi.org/10.1038/nature04245.
Huisman, J., Sharples, J., Stroom, J.M., Visser, P.M., Kardinaal, W.E.A., Verspagen, J.M.H., Sommeijer, B., 2004. Changes in turbulent mixing shift competition for light between phytoplankton species. Ecology. https://doi.org/10.1890/03-0763.
Iriarte, A., Daneri, G., Garcia, V.M.T., Purdie, D.A., Crawford, D.W., 1991. Plankton community respiration and its relationship to chlorophyll a concentrationinmarine coastal waters. Oceanol. Acta 14, 379–388.
Jago, C.F., Bale, A.J., Green, M.O., Howarth, M.J., Jones, S.E., McCave, I.N., Millward, G.E., Morris, A.W., Rowden, A.A., Williams, J.J., Hydes, D., Turner, A., Huntley, D., Leussen, W. Van, 1993. Resuspension processes and seston dynamics, southern north sea [and discussion]. Philos. Trans. Phys. Sci. Eng.
Jago, C.F., Jones, S.E., 1998. Observation and modelling of the dynamics of benthic fluff resuspended from a sandy bed in the southern North Sea. Cont. Shelf Res. 18, 1255–1282. https://doi.org/10.1016/S0278-4343(98)00043-0.
Jago, C.F., Jones, S.E., Latter, R.J., Mccandliss, R.R., Hearn, M.R., Howarth, M.J., 2002. Resuspension of benthic fluff by tidal currents in deep stratified waters, northern North Sea, 48, pp. 259–269.
Jakobsen, H.H., Markager, S., 2016. Carbon-to-chlorophyll ratio for phytoplankton in temperate coastal waters: seasonal patterns and relationship to nutrients. Limnol. Oceanogr. https://doi.org/10.1002/lno.10338.
Jenness, M.I., Duineveld, G.C.A., 1985. Effects of tidal currents on chlorophyll a content of sandy sediments in the southern North Sea. Mar. Ecol. Prog. Ser. 21, 283–287. https://doi.org/10.3354/meps021283.
Joint, I., Pomroy, A., 1993. Phytoplankton Biomass and Production in the Southern North-Sea. Mar. Ecol. Ser.
Jones, S.E., Jago, C.F., Bale, a.J., Chapman, D., Howland, R.J.M., Jackson, J., 1998. Aggregation and resuspension of suspended particulate matter at a stratified site in the southern North Sea: physical and biological controls. Cont. Shelf Res. 18, 1283–1309. https://doi.org/10.1016/S0278-4343(98)00044-2.
Kalaji, H.M., Schansker, G., Brestic, M., Bussotti, F., Calatayud, A., Ferroni, L., Goltsev, V., Guidi, L., Jajoo, A., Li, P., Losciale, P., Mishra, V.K., Misra, A.N., Nebauer, S.G., Pancaldi, S., Penella, C., Pollastrini, M., Suresh, K., Tambussi, E., Yanniccari, M., Zivcak, M., Cetner, M.D., Samborska, I.A., Stirbet, A., Olsovska, K., Kunderlikova, K., Shelonzek, H., Rusinowski, S., Bąba, W., 2017. Frequently asked questions about chlorophyll fluorescence, the sequel. Photosynth. Res. https://doi.org/10.1007/s11120-016-0318-y.
Kerimoglu, O., Hofmeister, R., Maerz, J., Riethmüller, R., Wirtz, K.W., 2017. The acclimative biogeochemical model of the southern North Sea. Biogeosciences 14 (19), 4499–4531. https://doi.org/10.5194/bg-14-4499-2017.
Kiefer, D.A., 1973. Chlorophyll a fluorescence in marine centric diatoms: responses of chloroplasts to light and nutrient stress. Mar. Biol. https://doi.org/10.1007/BF00394110.
Kononen, K., Hallfors, S., Kokkonen, M., Kuosa, H., Laanemets, J., Pavelson, J., Autio, R., 1998. Development of a subsurface chlorophyll maximum at the entrance to the Gulf of Finland, Baltic Sea. Limnol. Oceanogr. 43, 1089–1106. https://doi.org/10.4319/lo.1998.43.6.1089.
Krause, G., Budeus, G., Gerdes, D., Schaumann, K., Hesse, K., 1986. Frontal systems in the german bight and their physical and biological effects. Elsevier Oceanogr. Ser. 42, 119–140. https://doi.org/10.1016/S0422-9894(08)71042-0.
Kundu, P.K., Cohen, I.M., Dowling, D.R., 2016. Introduction (Chapter 1) In: Kundu, P.K., Cohen, I.M., Dowling, D.R. (Eds.), Fluid Mechanics, Sixth edition. Academic Press, Boston, pp. 1–48. https://doi.org/10.1016/B978-0-12-405935-1.00001-0. (Chapter 1).
Levandowsky, M., Kaneta, P.J., 1987. Behaviour in dinoflagellates. In: Taylor, F.J.R. (Ed.), The Biology of Dinoflagellates. Blackwell, Oxford, pp. 360–397.
Liu, Q., Kandasamy, S., Lin, B., Wang, H., Chen, C.-T.A., 2017. Biogeochemical characteristics of suspended particulates at deep chlorophyll maximum layers in the East China Sea. Biogeosciences. https://doi.org/10.5194/bg-15-2091-2018.
Löder, M.G.J., Kraberg, A.C., Aberle, N., Peters, S., Wiltshire, K.H., 2012. Dinoflagellates and ciliates at Helgoland Roads, North Sea. Helgol. Mar. Res. 66, 11–23. https://doi.org/10.1007/s10152-010-0242-z.
Lohse, L., Malschaert, J.F.P., Slomp, C.P., Helder, W., van Raaphorst, W., 1995. Sediment-water fluxes of inorganic nitrogen compounds along the transport route of organic matter in the North Sea. Ophelia. https://doi.org/10.1080/00785236.1995.10422043.
Lorenzen, C.J., 1966. A method for the continuous measurement of in vivo chlorophyll concentration. Deep Sea Res. Oceanogr. Abstr. https://doi.org/10.1016/0011-7471(66)91102-8.
Lutz, M., Dunbar, R., Caldeira, K., 2002. Regional variability in the vertical flux of particulate organic carbon in the ocean interior. Glob. Biogeochem. Cycles 16, 11–1-11–18. https://doi.org/10.1029/2000GB001383.
Macintyre, H.L., Kana, T.M., Geider, R.J., 2000. The effect of water motion on short-term rates of photosynthesis by marine phytoplankton. Trends Plant Sci. https://doi.org/10.1016/S1360-1385(99)01504-6.
Maerz, J., Hofmeister, R., Lee, E.M. Van Der, Gräwe, U., Riethmüller, R., Wirtz, W., 2016. Evidence for a maximum of sinking velocities of suspended particulate matter in a coastal transition zone. 〈https://doi.org/10.5194/bg-2015-667〉.
McCandliss, R.R., Jones, S.E., Hearn, M., Latter, R., Jago, C.F., 2002. Dynamics of suspended particles in coastal waters (southern North Sea) during a spring bloom. J. Sea Res. 47, 285–302. https://doi.org/10.1016/S1385-1101(02)00123-5.
McDougall, T.J., Feistel, Rainer, Wright, D.G., Pawlowicz, R., Millero, F.J., Jackett, D.R., King, B.A., Marion, G.M., Seitz, S., Spitzer, P., Chen, C.-T.A., 2010. The international thermodynamic equation of seawater - 2010: Calculation and use of thermodynamic properties, Intergovernmental Oceanographic Commission, Manuals and Guides No. 56. 〈https://doi.org/http://dx.doi.org/10.1109/VETECF.2008.21〉.
McTigue, N.D., Bucolo, P., Liu, Z., Dunton, K.H., 2015. Pelagic-benthic coupling, food webs, and organic matter degradation in the Chukchi Sea: insights from sedimentary pigments and stable carbon isotopes. Limnol. Oceanogr. https://doi.org/10.1002/lno.10038.
Millero, F.J., Feistel, R., Wright, D.G., McDougall, T.J., 2008. The composition of standard seawater and the definition of the reference-composition salinity scale. Deep. Res. Part I Oceanogr. Res. Pap. https://doi.org/10.1016/j.dsr.2007.10.001.
Millward, G.E., Morris, A.W., Tappin, A.D., 1998. Trace metals at two sites in the southern North Sea: results from a sediment resuspension study. Cont. Shelf Res. 18, 1381–1400. https://doi.org/10.1016/S0278-4343(98)00049-1.
Monismith, S.G., Koseff, J.R., White, B.L., 2018. Mixing efficiency in the presence of stratification: when is it constant? Geophys. Res. Lett. 45, 5627–5634. https://doi.org/10.1029/2018GL077229.
Müller, D., Krasemann, H., Brewin, R.J.W., Brockmann, C., Deschamps, P.Y., Doerffer, R., Fomferra, N., Franz, B.A., Grant, M.G., Groom, S.B., Mélin, F., Platt, T., Regner, P., Sathyendranath, S., Steinmetz, F., Swinton, J., 2015. The Ocean Colour Climate Change Initiative: II. Spatial and temporal homogeneity of satellite data retrieval due to systematic effects in atmospheric correction processors. Remote Sens. Environ. https://doi.org/10.1016/j.rse.2015.01.033.
Nielsen, L.T., Kiørboe, T., 2015. Feeding currents facilitate a mixotrophic way of life. ISME J. 9, 2117–2127. https://doi.org/10.1038/ismej.2015.27.
Nielsen, T.G., Lokkegaard, B., Richardson, K., Pedersen, F.B., Hansen, L., 1993. Structure of plankton communities in the Dogger Bank area (North Sea) during a stratified situation. Mar. Ecol. Prog. Ser. 95, 115–131. https://doi.org/10.3354/meps095115.
Omand, M.M., Mahadevan, A., 2015. The shape of the oceanic nitracline. Biogeosciences 12, 3273–3287. https://doi.org/10.5194/bg-12-3273-2015.
Osborn, T.R., 1980. Estimates of the local rate of vertical diffusion from dissipation

measurements. J. Phys. Oceanogr. https://doi.org/10.1175/1520-0485(1980)010<0083:EOTLRO>2.0.CO;2.
Otto, L., Zimmerman, J.T.F., Furnes, G.K., Mork, M., Saetre, R., Becker, G., 1990. Review of the physical oceanography of the North Sea. Netherlands. J. Sea Res. 26, 161–238. https://doi.org/10.1016/0077-7579(90)90091-T.
Pedersen, F.B., 1994. The oceanographic and biological tidal cycle succession in shallow sea fronts in the north sea and the english channel. Estuar. Coast. Shelf Sci. 38, 249–269. https://doi.org/10.1006/ecss.1994.1017.
Peeters, J.C.H., Los, F.J., Jansen, R., Haas, H.A., Peperzak, L., de Vries, I., 1995. The oxygen dynamics of the oyster ground, north sea. Impact eutrophication Environ. Cond. Ophelia. https://doi.org/10.1080/00785326.1995.10431508.
Petersen, W., Schroeder, F., Bockelmann, F.D., 2011. FerryBox - Application of continuous water quality observations along transects in the North Sea. Ocean Dyn. 61, 1541–1554. https://doi.org/10.1007/s10236-011-0445-0.
Pingree, R.D., Griffiths, D.K., 1978. Tidal fronts on the shelf seas around the British Isles. J. Geophys. Res. 83, 4615. https://doi.org/10.1029/JC083iC09p04615.
Pohlmann, T., 1996a. Calculating the development of the thermal vertical stratification in the North Sea with a three-dimensional baroclinic circulation model. Cont. Shelf Res. https://doi.org/10.1016/0278-4343(95)00018-V.
Pohlmann, T., 1996b. Predicting the thermocline in a circulation model of the North Sea - Part I: model description, calibration and verification. Cont. Shelf Res. 16, 131–146. https://doi.org/10.1016/0278-4343(95)90885-S.
Provoost, P., Braeckman, U., Van Gansbeke, D., Moodley, L., Soetaert, K., Middelburg, J.J., Vanaverbeke, J., 2013. Modelling benthic oxygen consumption and benthic-pelagic coupling at a shallow station in the southern North Sea. Estuar. Coast. Shelf Sci. 120, 1–11. https://doi.org/10.1016/j.ecss.2013.01.008.
Richardson, K., Pedersen, F.B., 1998. Estimation of new production in the North Sea : consequences for temporal and spatial variability of phytoplankton, pp. 574–580.
Richardson, K., Visser, A.W., Bo Pedersen, F., 2000. Subsurface phytoplankton blooms fuel pelagic production in the North Sea. J. Plankton Res 22, 1663–1671. https://doi.org/10.1093/plankt/22.9.1663.
Riley, G.A., 1942. The relationship of vertical turbulence and spring diatom flowerings. J. Mar. Res. 5, 67–87.
Rumyantseva, A., Lucas, N., Rippeth, T., Martin, A., Painter, S.C., Boyd, T.J., Henson, S., 2015. Ocean nutrient pathways associated with the passage of a storm. Glob. Biogeochem. Cycles 29, 1179–1189. https://doi.org/10.1002/2015GB005097.
Russell, F.S., 1927. The vertical distribution of plankton in the sea. Biol. Rev. 213–262. https://doi.org/10.1111/j.1469-185X.1927.tb00878.x.
Saha, S., Moorthi, S., Pan, H.L., Wu, X., Wang, J., Nadiga, S., Tripp, P., Kistler, R., Woollen, J., Behringer, D., Liu, H., Stokes, D., Grumbine, R., Gayno, G., Wang, J., Hou, Y.T., Chuang, H.Y., Juang, H.M.H., Sela, J., Iredell, M., Treadon, R., Kleist, D., Van Delst, P., Keyser, D., Derber, J., Ek, M., Meng, J., Wei, H., Yang, R., Lord, S., Van Den Dool, H., Kumar, A., Wang, W., Long, C., Chelliah, M., Xue, Y., Huang, B., Schemm, J.K., Ebisuzaki, W., Lin, R., Xie, P., Chen, M., Zhou, S., Higgins, W., Zou, C.Z., Liu, Q., Chen, Y., Han, Y., Cucurull, L., Reynolds, R.W., Rutledge, G., Goldberg, M., 2010. The NCEP climate forecast system reanalysis. Bull. Am. Meteorol. Soc. https://doi.org/10.1175/2010BAMS3001.1.
Schrum, C., 1997. Thermohaline stratification and instabilities at tidal mixing fronts: results of an eddy resolving model for the German Bight. Cont. Shelf Res. 17, 689–716. https://doi.org/10.1016/S0278-4343(96)00051-9.
Schrum, C., Hübner, U., Jacob, D., Podzun, R., 2003a. A coupled atmosphere/ice/ocean model for the North Sea and the Baltic Sea. Clim. Dyn. https://doi.org/10.1007/s00382-003-0322-8.
Schrum, C., Siegismund, F., John, M.S., 2003b. Decadal variations in the stratification and circulation patterns of the North Sea. Are the 1990s unusual? ICES Mar. Sci. Symp. 219, 121–131.
Schrum, C., St. John, M., Alekseeva, I., 2006. ECOSMO, a coupled ecosystem model of the North Sea and Baltic Sea: Part II. Spatial-seasonal characteristics in the North Sea as revealed by EOF analysis. J. Mar. Syst. 61, 100–113. https://doi.org/10.1016/j.jmarsys.2006.01.004.
Schultze, L.K.P., Merckelbach, L.M., Carpenter, J.R., 2017. Turbulence and mixing in a shallow shelf sea from underwater gliders. J. Geophys. Res. Ocean. 9092–9109. https://doi.org/10.1002/2017JC012872.
Scott, B.E., Sharples, J., Ross, O.N., Wang, J., Pierce, G.J., Camphuysen, C.J., 2010. Subsurface hotspots in shallow seas: fine-scale limited locations of top predator foraging habitat indicated By tidal mixing and sub-surface chlorophyll. Mar. Ecol. Prog. Ser. 408, 207–226. https://doi.org/10.3354/meps08552.
Sharples, J., 2008. Potential impacts of the spring-neap tidal cycle on shelf sea primary production. J. Plankton Res. 30, 183–197. https://doi.org/10.1093/plankt/fbm088.
Sharples, J., Moore, M.C., Rippeth, T.P., Holligan, P.M., Hydes, D.J., Fisher, N.R., Simpson, J.H., 2001. Phytoplankton distribution and survival in the thermocline. Limnol. Oceanogr. https://doi.org/10.4319/lo.2001.46.3.0486.
Sharples, J., Tweddle, J.F., Green, J.A.M., Palmer, M.R., Kim, Y., Hickman, A.E., Holligan, P.M., Moore, C.M., Rippeth, T.P., Simpson, J.H., Krivtsov, V., 2007. Spring – neap modulation of internal tide mixing and vertical nitrate fluxes at a shelf edge in summer, 52, pp. 1735–1747.
Simpson, J., J.H.S, 2012. Introduction to the Physical and Biological Oceanography of Shelf Seas. Cambridge University Presshttps://doi.org/10.1017/CBO9781139034098.
Simpson, J.H., Hunter, J.R., 1974. Fronts in the Irish Sea. Nature 250, 404–406. https://doi.org/10.1038/250404a0.
Simpson, J.H., Sharples, J., Rippeth, T.P., 1991. A prescriptive model of stratification induced by freshwater runoff. Estuar. Coast. Shelf Sci. 33, 23–35. https://doi.org/10.1016/0272-7714(91)90068-M.
Smayda, T.J., 1971. Normal and accelerated sinking of phytoplankton in the sea. Mar. Geol. https://doi.org/10.1016/0025-3227(71)90070-3.
Smith, C., DeMaster, D., Thomas, C., Srsen, P., Grange, L., Evrard, V., DeLeo, F., 2012. Pelagic-benthic coupling, food banks, and climate change on the west antarctic peninsula shelf. Oceanography. https://doi.org/10.5670/oceanog.2012.94.
Steele, J.H., Yentsch, C.S., 1960. The vertical distribution of chlorophyll. J. Mar. Biol. Assoc. https://doi.org/10.1017/S0025315400013266.
Steinbuck, J.V., Genin, A., Monismith, S.G., Koseff, J.R., Holzman, R., Labiosa, R.G., 2010. Turbulent mixing in fine-scale phytoplankton layers: observations and inferences of layer dynamics. Cont. Shelf Res. 30, 442–455. https://doi.org/10.1016/j.csr.2009.12.014.
Stramska, M., Stramski, D., 2005. Effects of a nonuniform vertical profile of chlorophyll concentration on remote-sensing reflectance of the ocean. Appl. Opt. https://doi.org/10.1364/AO.44.001735.
Su, J., Tian, T., Krasemann, H., Schartau, M., Wirtz, K., 2015. Response patterns of phytoplankton growth to variations in resuspension in the German Bight revealed by daily MERIS data in 2003 and 2004. Oceanologia. https://doi.org/10.1016/j.oceano.2015.06.001.
Suess, E., 1980. Particulate organic carbon flux in the oceans - surface productivity and oxygen utilization. Nature. https://doi.org/10.1038/288260a0.
Swinehart, D.F., 1962. The Beer-Lambert law. J. Chem. Educ. https://doi.org/10.1021/ed039p333.
Thompson, C.E.L., Couceiro, F., Fones, G.R., Helsby, R., Amos, C.L., Black, K., Parker, E.R., Greenwood, N., Statham, P.J., Kelly-Gerreyn, B.A., 2011. In situ flume measurements of resuspension in the North Sea. Estuar. Coast. Shelf Sci. https://doi.org/10.1016/j.ecss.2011.05.026.
Wang, X.J., Behrenfeld, M., Le Borgne, R., Murtugudde, R., Boss, E., 2009. Regulation of phytoplankton carbon to chlorophyll ratio by light, nutrients and temperature in the equatorial pacific ocean: a basin-scale model. Biogeosciences. https://doi.org/10.5194/bg-6-391-2009.
Westernhagen, H., Hickel, W., Bauerfeind, E., Niermann, U., Kröncke, I., 1986. Sources and effects of oxygen deficiencies in the south-eastern North Sea. Ophelia 26, 457–473. https://doi.org/10.1080/00785326.1986.10422006.
Weston, K., Fernand, L., Mills, D.K., Delahunty, R., Brown, J., 2005. Primary production in the deep chlorophyll maximum of the central North Sea. J. Plankton Res. 27, 909–922. https://doi.org/10.1093/plankt/fbi064.
Williams, C., Sharples, J., Mahaffey, C., Rippeth, T., 2013. Wind-driven nutrient pulses to the subsurface chlorophyll maximum in seasonally stratified shelf seas. Geophys. Res. Lett. 40, 5467–5472. https://doi.org/10.1002/2013GL058171.
Xing, X., Morel, A., Claustre, H., D'Ortenzio, F., Poteau, A., 2012. Combined processing and mutual interpretation of radiometry and fluorometry from autonomous profiling Bio-Argo floats: 2. Colored dissolved organic matter absorption retrieval. J. Geophys. Res. Ocean. 117, 1–14. https://doi.org/10.1029/2011JC007632.
Yacobi, Y.Z., 2006. Temporal and vertical variation of chlorophyll a concentration, phytoplankton photosynthetic activity and light attenuation in Lake Kinneret: possibilities and limitations for simulation by remote sensing. J. Plankton Res. https://doi.org/10.1093/plankt/fbl004.
Zhang, W., Wirtz, K., 2017. Mutual dependence between sedimentary organic carbon and infaunal macrobenthos resolved by mechanistic modeling. J. Geophys. Res. Biogeosci. 122, 2509–2526. https://doi.org/10.1002/2017JG003909.
Zhao, C., Daewel, U., Schrum, C., 2018. Tidal impacts on primary production in the North Sea. Earth Syst. Dyn. Discuss. 1–44. https://doi.org/10.5194/esd-2018-74.